805 MHz $\beta = 0.47$ Elliptical Accelerating Structure R & D: Final Report DE-FG02-03ER41247

S. Bricker, C. Compton, T. Grimm[*], W. Hartung, M. Johnson, F. Marti,
H. Podlech[†], J. Popierlarski, R. C. York,
National Superconducting Cyclotron Laboratory, Michigan State University,
East Lansing, Michigan
G. Ciovati, P. Kneisel, L. Turlington
Thomas Jefferson National Accelerator Facility, Newport News, Virginia
D. Barni, C. Pagani, P. Pierini
INFN Milano—Laboratorio LASA, Segrate (Milano), Italy

22 September 2008

Abstract

A 6-cell 805 MHz superconducting cavity for acceleration in the velocity range of about 0.4 to 0.53 times the speed of light was designed. After single-cell prototyping, three 6-cell niobium cavities were fabricated. In vertical RF tests of the 6-cell cavities, the measured quality factors (Q_0) were between $7 \cdot 10^9$ and $1.4 \cdot 10^{10}$ at the design field (accelerating gradient of 8 to 10 MV/m). A rectangular cryomodule was designed to house 4 cavities per cryomodule. The 4-cavity cryomodule could be used for acceleration of ions in a linear accelerator, with focussing elements between the cryomodules. A prototype cryomodule was fabricated to test 2 cavities under realistic operating conditions. Two of the 6-cell cavities were equipped with helium tanks, tuners, and input coupler and installed into the cryomodule. The prototype cryomodule was used to verify alignment, electromagnetic performance, frequency tuning, cryogenic performance, low-level RF control, and control of microphonics.

[*]Present address: Niowave, Inc., 1012 North Walnut St, Lansing, Michigan 48906 USA
[†]Present address: Institut für Angewandte Physik, Goethe-Universität, Frankfurt am Main, Germany.

Contents

1 Introduction

Superconducting accelerators are presently used to accelerate particles that are light enough to have $v/c \equiv \beta \approx 1$ (electrons and positrons), or heavy enough (ions) to have $\beta \ll 1$ (where v is the beam velocity and c is the speed of light). Historically, superconducting cavities have not been used in between these two extremes. New cavity designs are being developed span this gap: in recent years, a number of superconducting accelerators have been proposed to accelerate particles all the way from very low β to β close to 1.

To achieve this, the traditional low-β structures (quarter-wave resonators and variants thereof, typically used for $\beta \leq 0.2$) are being doubled up (into half-wave resonators and variants thereof) to be used for higher β values. Likewise, the traditional $\beta = 1$ structures (axisymmetric cavities of elliptical cross-section) are being shortened for use at lower β values.

The development of elliptical cavities for $\beta < 1$ was pioneered at Los Alamos, where the original goal was a 1 GeV pion linac, PILAC [1]. It was realised from the beginning that it is better to use a few different cavity shapes, each optimised for one specific β value, rather than making each cavity in the accelerator unique to the exact β of the beam at the location of the cavity; the advantages of simplified cavity fabrication and increased flexibility for installation and operation more than make up for the fact that the cavity voltages are not used with complete efficiency everywhere along the accelerator.

Although PILAC did not come to fruition, the original concept was adopted to a number of other projects. A number of lower-β elliptical cavity prototypes have now been built by various laboratories [2, 3, 4, 5, 6, 7, 8, 9, 10]. Moreover, the Spallation Neutron Source (SNS) is using superconducting elliptical cavities with $\beta = 0.61$ and $\beta = 0.81$ for the SNS linac. The successful results with multi-cell cavities for SNS [11], as well as several other projects [6, 7, 8, 9], provide a good basis for this technology choice.

Although SNS uses normal conducting cavities for velocities below the reach of the SNS $\beta = 0.61$ cavity, single-cell prototypes of elliptical cavities for even lower β values have been prototyped at several laboratories: two $\beta = 0.48$ cavities (700 MHz) were tested by Los Alamos [2]; a $\beta = 0.45$ cavity (1.3 GHz) was tested by KEK [3]; two $\beta = 0.5$ cavities (600 MHz) were tested by JAERI [4]; a $\beta = 0.47$ cavity (700 MHz) was tested by INFN-Milano and Saclay [10]. Encouragingly, the desired gradients and quality factors were exceeded in all of these single-cell tests.

A 5-cell $\beta = 0.5$ cavity prototype (600 MHz) was also tested by JAERI and KEK [7]. Good low-field performance was ultimately achieved [12]. The high-field performance was not as good as expected, but this was not attributed to anything intrinsic to the low β.

In light of the promising results with elliptical cavities for β in the vicinity of 0.5, a medium-β multi-cell cavity and cryomodule development program was undertaken as a collaboration between INFN-Milano, Jefferson Lab, and the National Superconducting Cyclotron Laboratory (NSCL) at Michigan State University (MSU). The work was carried out as part of the design of the driver linac for a proposed accelerator for rare isotope beams. The driver linac would provide an intense beam of exotic isotopes for nuclear physics re-

search. It would accelerate heavy ions to high energy (200 MeV per nucleon or higher), with a high beam power (up to 400 kW). In order to maximise the beam power, the driver linac would operate continuously, making it advantageous for the entire linac to be superconducting. Quarter-wave and half-wave resonators would be used for the low-β portion of the linac; elliptical cavities, including the $\beta = 0.61$ and $\beta = 0.81$ SNS cavities, could be used for the high-energy portion. Though the present development effort is for heavy ion beams, the $\beta = 0.47$ technology could also be applied to superconducting linacs for proton or H^- beams, several of which have been proposed [13, 14].

A rectangular cryomodule design was developed for the $\beta_g = 0.47$ elliptical cavities. With minor variations, the design could accommodate all of the superconducting cavity and magnet types needed for a 400 kW heavy ion linac. The rectangular cryomodule is more compact than the SNS cryomodule, allowing for a smaller tunnel cross-section and a higher real estate gradient. The cold mass alignment is accomplished with titanium rails supported by adjustable nitronic links, similar to the alignment system used for superconducting magnet cryostats at MSU.

A prototype cryomodule for the $\beta_g = 0.47$ elliptical cavities was designed and fabricated. The prototype contains 2 multi-cell cavities instead of the 4 cavities planned for production cryomodules, since the critical issues of cavity gradient, quality factor, and microphonics (which drive the linac cost via module count, cryo-plant capacity, and RF amplifier power) can be addressed with 2 cavities. Cryogenic and RF testing of the prototype cryomodule were done. Alignment of the cold mass, cryogenic performance of the cryomodule, RF performance of the cavities and couplers, and frequency tuning of the cavities was verified. Measurements on microphonics and microphonics control for the cryomodule cavities were also done [15, 16].

This report covers the design of the 6-cell $\beta = 0.47$ cavity, the fabrication of prototype cavities, vertical RF tests on single-cell prototypes and multi-cell prototypes, the design of the prototype cryomodule, and the testing of the prototype cryomodule. More complete information on the single-cell results may be found in previous papers [17, 18]. Results on the multi-cell cavity vertical tests have also been previously reported [19, 20]. Additional papers have been published on the cryomodule design [21] and on the measurements on the prototype cryomodule [22].

2 Cavity Design

Let us define the maximum $\beta \equiv \beta_m$ to be the β value for which the beam receives the maximum accelerating kick from the actual cavity, and the geometric $\beta \equiv \beta_g$ to be the maximum β value in the case of a periodic structure, i.e. a multi-cell structure in the limit of an arbitrarily large number of cells. For the obvious reasons, the latter quantity is usually referred to for high-β cavities, while the former quantity (also called "optimum β") is usually given for low-β cavities.

The SNS $\beta_g = 0.81$ and $\beta_g = 0.61$ cavities are the basis for the $\beta_g = 0.47$ cell shape [17, 23]. The $\beta_g = 0.47$ cell shape is compared with those of the SNS cavities and the TeSLA

Test Facility (TTF) cavity [24] in Figure 1. As can be seen, the $\beta_g = 0.47$ cell shape is relatively close to the $\beta_g = 0.61$ cell shape. Thus, stiffening and bracing techniques being used for the SNS cavities can be applied to the $\beta_g = 0.47$ cavity also.

As indicated above, medium-β cavities must accelerate a beam whose velocity is varying with position. The penalty due to the velocity mismatch can be quantified via the transit time factor (the maximum energy gain for a particle travelling at speed βc divided by the energy gain for the ideal case in which the field's time variation is not accounted for and the phase is optimal at every point along the particle's path). The transit time factor of the $\beta_g = 0.47$ cavity is shown in Figure 2 for the 6-cell case and two other cases. The transit time factor was calculated with SUPERFISH [25, 26].

The approximate range of usefulness of the 6-cell cavity is from $\beta = 0.4$ to $\beta = 0.53$ (indicated by dotted lines in Figure 2). The useful range is not determined by the cavity characteristics alone; if the $\beta_g = 0.47$ cavity is used in a linac with different cavity geometries

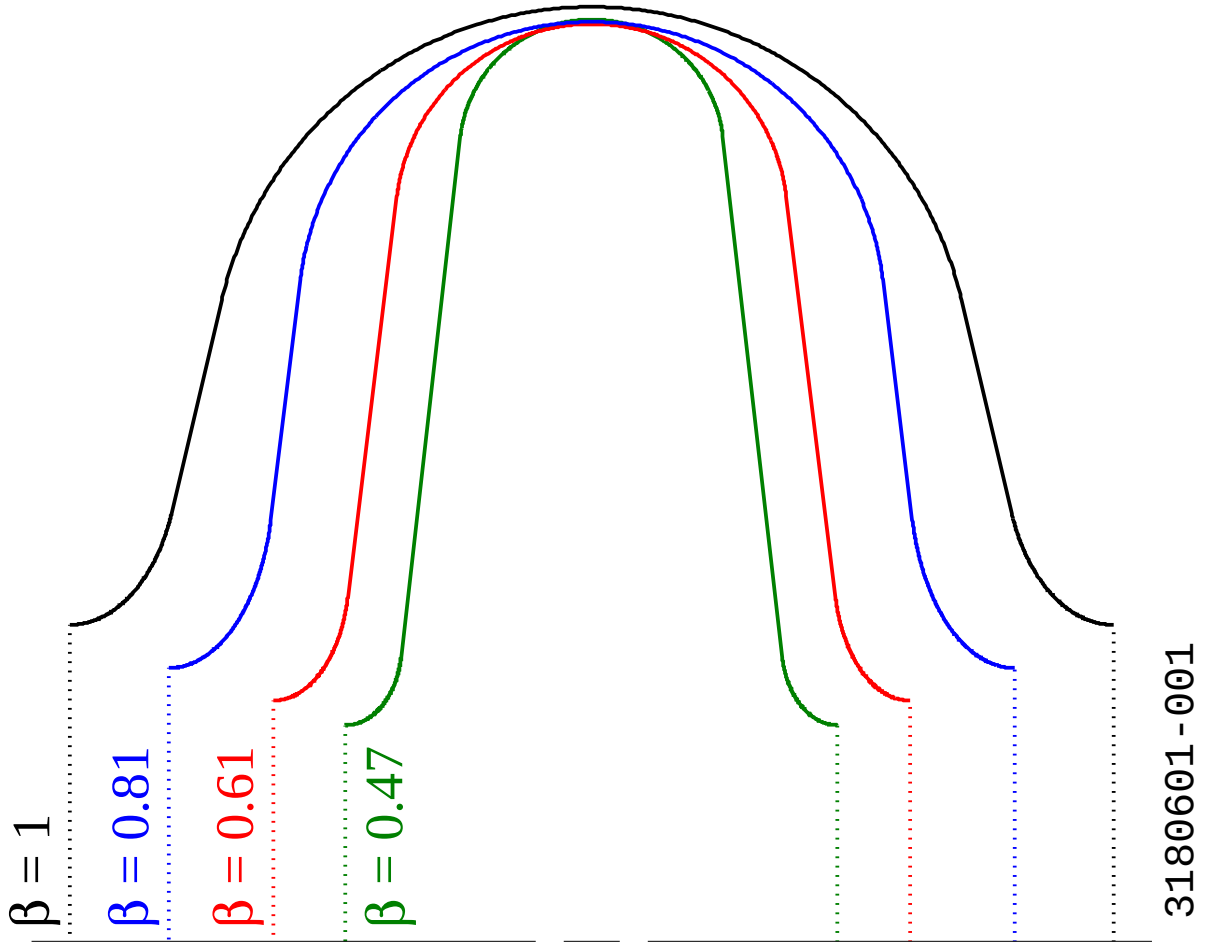

Figure 1. Comparison of the $\beta_g = 0.47$ cell with a $\beta_g = 0.61$ cell (SNS), a $\beta_g = 0.81$ cell (SNS), and a $\beta_g = 1$ cell (TTF, scaled to 805 MHz).

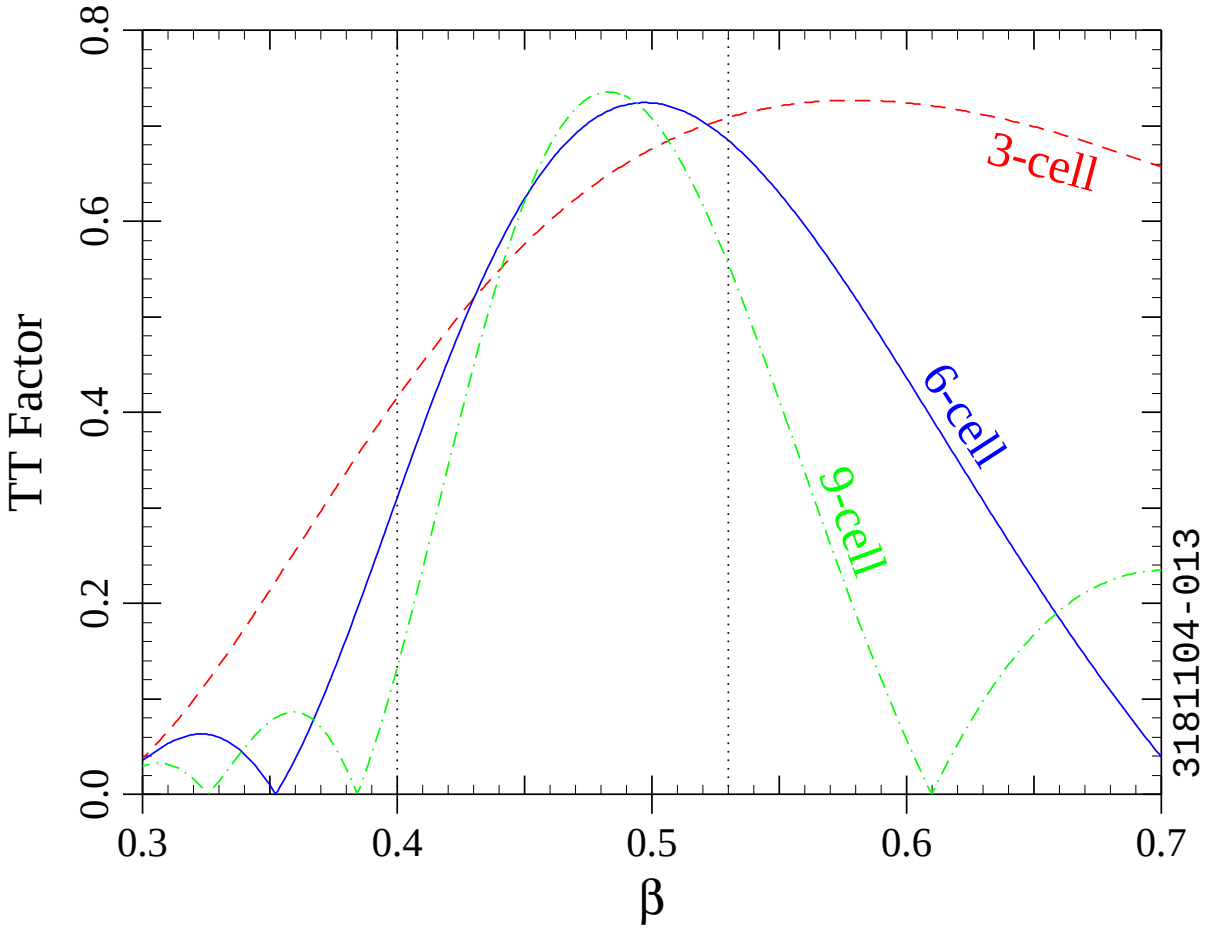

Figure 2. Dependence of the transit time factor on β for the $\beta_g = 0.47$ cavity for 3 cells, 6 cells, and 9 cells.

upstream and downstream of it, the useful velocity range is determined from the velocities at which one cavity geometry becomes more efficient than another.

The choice of 6 cells is a reasonable compromise between a long structure to provide higher voltage and a small number of cells for higher velocity acceptance. Note that β_m is between 0.49 and 0.50 in the 6-cell case, i.e. slightly larger than β_g; particles with β slightly larger than β_g acquire a little more energy travelling through the cavity and suffer less deceleration from the evanescent field in the beam tube. As can be seen in Figure 2, the discrepancy between β_g and β_m becomes more pronounced as the number of cells is reduced.

The beam tube is enlarged on one side of the SNS cavities to provide stronger input coupling. Less coupling is needed for a heavy ion linac, so no enlargement of the beam tube is required for the $\beta_g = 0.47$ cavity [27]. This simplifies the cavity fabrication and yields a slight improvement in the RF parameters of the structure. Selected cavity parameters are

given in Table 1. The accelerating mode is a standing-wave mode, as is the case for most superconducting cavities. In Table 1, E_p and B_p are the peak surface electric and magnetic field, respectively; R_a is the shunt impedance (linac definition) and E_a is the accelerating gradient (both include the transit time factor with $\beta = \beta_g$). The RF parameters in Table 1 were calculated with SUPERFISH [25, 26] and checked with SuperLANS [28].

An analysis was done of the excitation of higher-order modes (HOMs) in the cavity by the beam and coupling of the HOMs to the input coupler and pick-up antenna. This analysis indicates that HOM couplers are not required for operation of the $\beta_g = 0.47$ cavity in a heavy ion linac, allowing for further simplification of the system [27].

Table 1. Parameters of the symmetric 6-cell $\beta_g = 0.47$ cavity. RF quantities were calculated with SUPERFISH.

Cell mode	TM_{010}
Phase advance per cell	π
Resonant frequency f	805 MHz
Cell-to-cell coupling $\equiv 2(f_\pi - f_0)/(f_\pi + f_0)$	1.5%
E_p/E_a	3.34
cB_p/E_a	1.98
R_a/Q	173 Ω
Geometry factor G	136 Ω
Active length $\equiv 6\beta_g c/(2f)$	527 mm
Inner diameter at iris (aperture)	77.2 mm
Inner diameter at equator	329 mm

3 Single-Cell Cavity Prototyping

Two single-cell prototypes of the $\beta_g = 0.47$ cavity were fabricated and tested. Some of the results are shown in Figure 3. The highest gradient reached in the first round of tests [17] was about 15 MV/m. As can be seen in Figure 3, the Q_0 values at 15 MV/m were about 10^{10}; the low-field Q_0 values were between $2 \cdot 10^{10}$ and $4 \cdot 10^{10}$. These measurements were done at 2 K in a vertical cryostat at Jefferson Lab.

A number of additional tests were done on the second of the two single-cell cavities while commissioning the facilities at MSU for etching, high-pressure rinsing, clean assembly, RF testing, and helium processing of superconducting cavities. The highest gradient reached in these tests was about 18 MV/m, albeit with a slightly lower Q_0; nevertheless, Q_0 still exceeded 10^{10} at $E_a = 10$ MV/m [18]. As can be seen in Figure 3, some improvement in the low-field Q_0 was seen at temperatures below 2 K, but the high-field performance did not change much.

More detailed information on the single-cell results may be found elsewhere [17, 18].

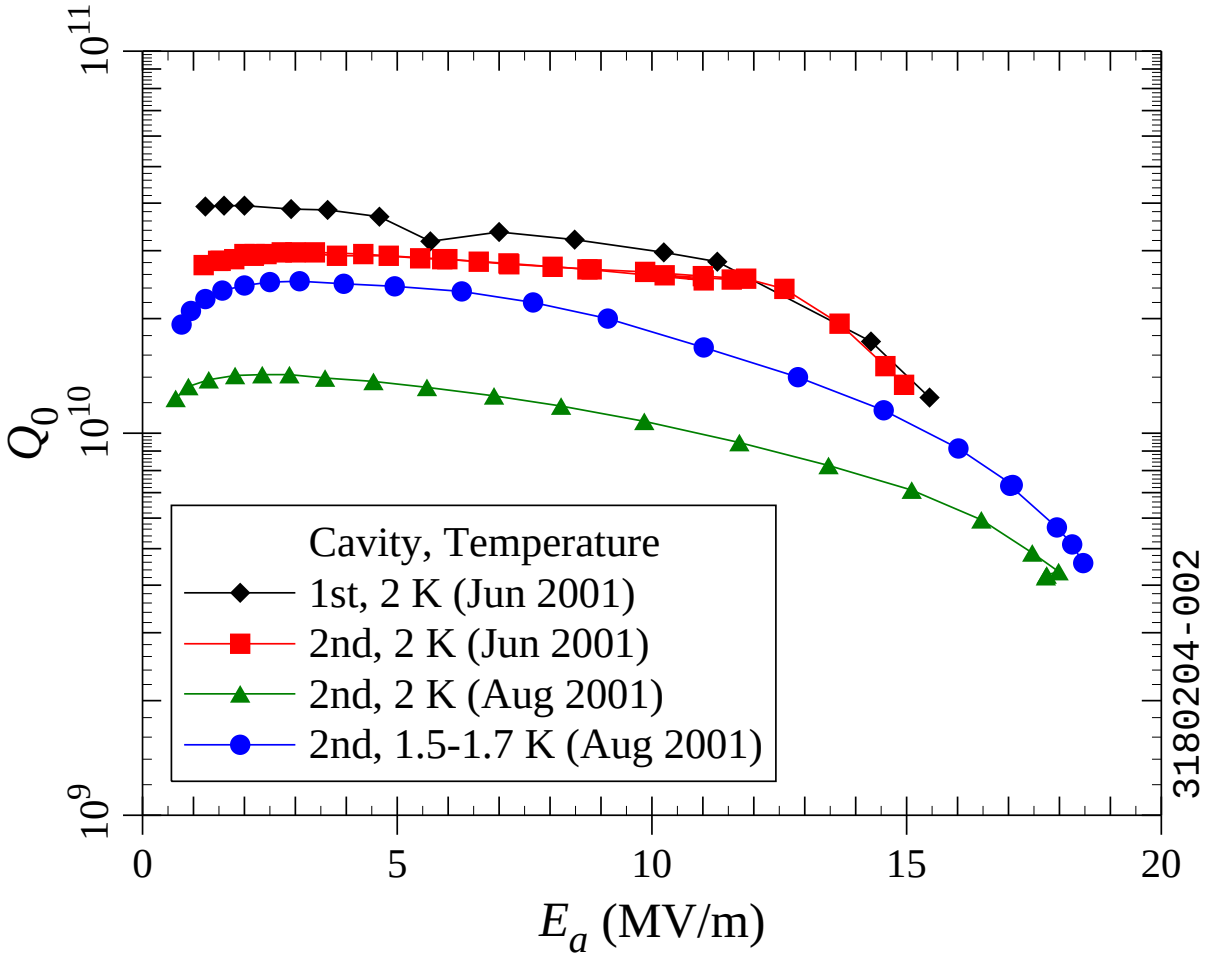

Figure 3. Measured dependence of the quality factor on the accelerating gradient for the single-cell cavity prototypes. The June 2001 measurements were done at Jefferson Lab; the August 2001 measurements were done at MSU. In the June 2001 tests, there may have been some RF conditioning during the measurements, as evidenced by a slight decrease and recovery in Q_0 at 6 to 7 MV/m (1st cavity) or 11 to 12 MV/m (2nd cavity).

4 Multi-Cell Cavity Prototyping

4.1 Cu Cavity

A copper multi-cell cavity was fabricated to check the procedures for forming and electron beam welding, and to make sure the desired frequency and field flatness could be obtained. Before field flatness tuning, the accelerating mode frequency of the copper model was 805.9 MHz; the initial electric field unflatness parameter ($\Delta E/E$) was 44%. The field flatness tuning was done using a tuning jig developed for the SNS cavities. The unflatness parameter was 7% after one iteration of flatness tuning. Thus, the initial frequency error was well

within the range of the tuning fixture, and the field flatness tuning was not a problem. The copper model was also used for higher-order mode and input coupling measurements [27].

4.2 Nb Cavity Fabrication and Preparation

The results on the copper model being satisfactory, three multi-cell niobium prototypes were fabricated next. The first 6-cell cavity (Figure 4) was a simplified version without stiffening rings, dishes for attachment of the helium vessel, or side ports for the RF couplers; these features were included in the second and third cavities (Figure 5).

Sheet Nb of thickness 4 mm with nominal Residual Resistivity Ratio (RRR) of 250 was used for all three cavities. The forming of half-cells and joining were done by the standard deep drawing and electron beam welding techniques used for elliptical cavities, including SNS prototype cavities fabricated at Jefferson Laboratory. As with the SNS cavities, Nb-Ti alloy flanges and Al alloy gaskets were used for the vacuum seal on the beam tubes.

The completed 6-cell cavities were etched with 1:1:1 Buffered Chemical Polishing solution (mixture of concentrated phosphoric acid, hydrofluoric acid, and nitric acid in equal parts by volume). About 100 μm was removed from the inside surface of the first Nb multi-cell. The cavity was then fired in a vacuum furnace for 10 hours at 600°C to remove hydrogen and prevent subsequent formation of lossy surface hydrides—in other words, to inoculate it against "Q disease" [29]. The pressure in the furnace was $\leq 10^{-6}$ torr during the heat treatment. Field flatness tuning was done next. The final preparation steps were etching of an additional 60 μm from the inner surface and high-pressure rinsing with ultra-pure water

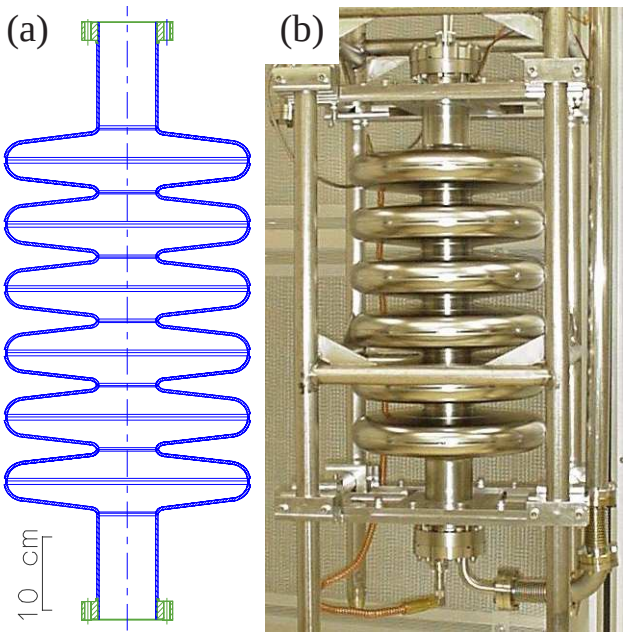

Figure 4. (a) Drawing of the first six-cell $\beta_g = 0.47$ cavity and (b) photograph of the cavity on the insert. In (a), Nb parts are in blue and Nb-Ti parts are in green.

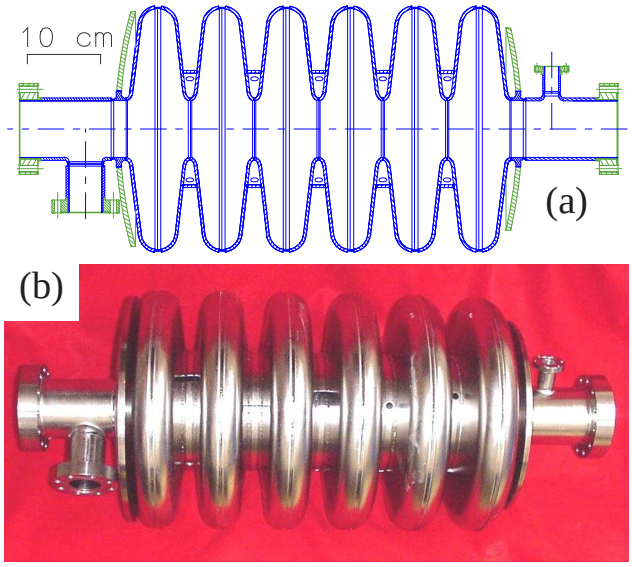

Figure 5. (a) Drawing of the second and third six-cell $\beta_g = 0.47$ Nb cavities and (b) photograph of the second cavity. The port for the input coupler can be seen on the left beam tube. Rings are welded around the outside of the irises to increase the mechanical stiffness of the structure. The end dishes for the attachment of the helium vessel are also visible.

in a clean room to remove particulates from the inside surface of the cavity. No vacuum bake-out was done after assembly of the cavity onto the insert.

About 150 μm was removed during the etch of the second cavity; additional etching was done after the first RF test, as will be described below. About 300 μm was removed from the third cavity in 2 etching cycles. The second and third cavities were rinsed with high-pressure water, but no firing was done. The third cavity was rinsed twice, as a leak was found in the input coupler port after the first rinse.

4.3 Field Flatness Tuning

Field flatness tuning was done on all three niobium cavities. The goal was a field unflatness parameter ($\Delta E/E$) of 10% or less. The first cavity was tuned with the SNS tuning jig, as had been done with the copper model. After tuning, $\Delta E/E$ was 12%. The tuning was more difficult than it had been with the copper cavity. The second and third Nb cavities were tuned with a new custom-built jig for the $\beta_g = 0.47$ cavity. This made the tuning easier; with the second Nb cavity, $\Delta E/E = 5\%$ was reached in one iteration (see Figure 6). The results on the third cavity were similar ($\Delta E/E = 4.5\%$).

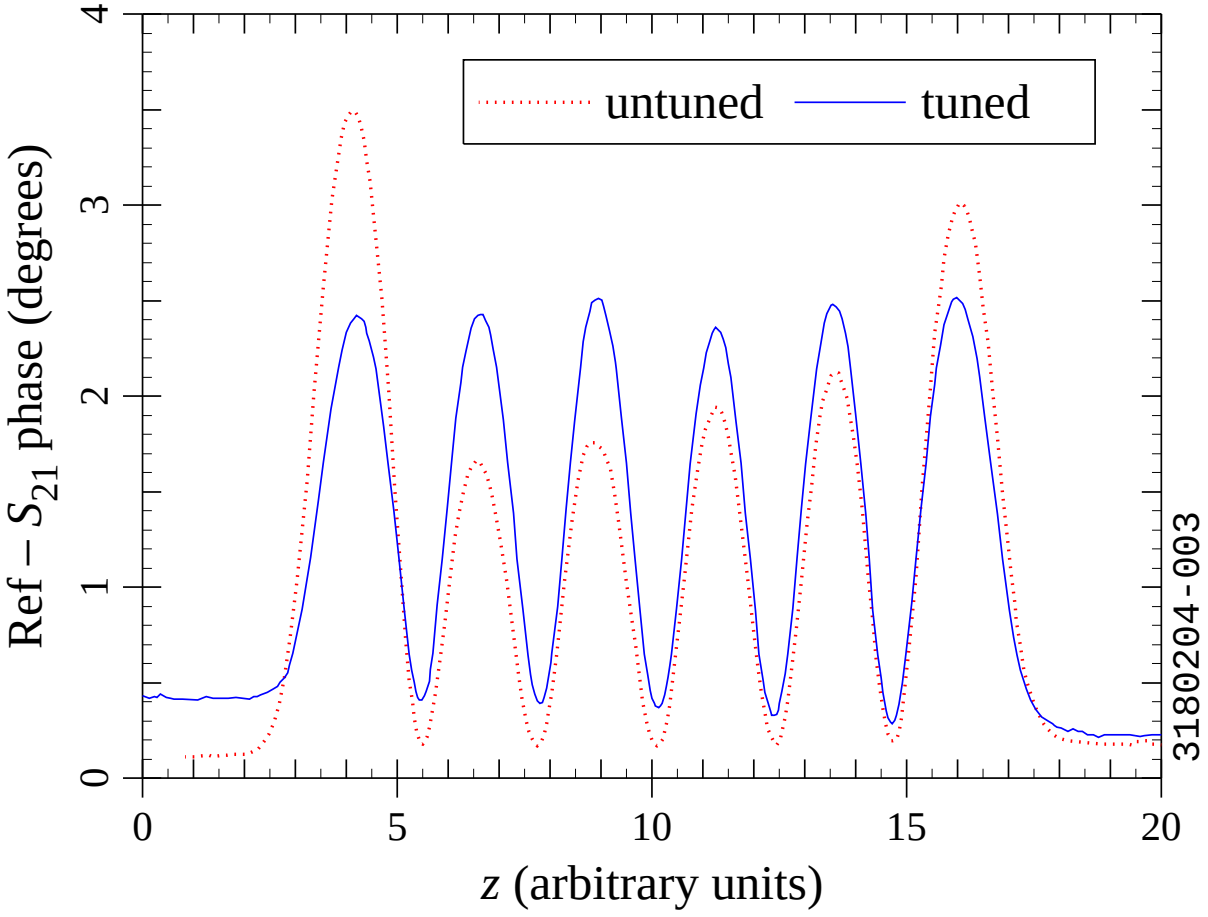

Figure 6. Bead pulls for the second six-cell niobium cavity. The phase shift (proportional to the square of the electric field) as a function of bead position z was measured with a network analyser.

5 Vertical RF Testing of Multi-Cell Cavities

RF tests were done on all three cavities in a vertical cryostat. The residual magnetostatic field inside the cryostat was less than 1 μT. In all cases, the cryostat was cooled down rapidly to 4.3 K and then pumped to 2 K. The RF power was supplied by a 500 W amplifier; a phase feedback loop was used to make sure that the cavity was always driven on resonance. Copper probe antennae on the beam tube end-cap flanges (fixed coupling strength) were used for the input coupler and pick-up. A radiation sensor on top of the insert was used to monitor x-rays during the RF tests. Radiation shielding surrounded the cryostat during all RF testing.

5.1 First Test on the First Cavity

The first vertical RF test was done on the first cavity in September 2002. Figure 7 (squares) shows the measurement of the quality factor as a function of field level. As can be seen, the low-field Q_0 was about $2 \cdot 10^{10}$ and Q_0 remained above 10^{10} up to $E_a \approx 11$ MV/m. A gradient of about 16 MV/m was reached. The test was stopped at that level due to the failure of an RF cable. Some x-rays were observed at high field (0.7 rem/hour), indicating that the decrease in Q_0 at high field was likely due to field emission. Modest RF conditioning (with radiation levels up to 1.2 rem/hour) was required to reach a gradient of 16 MV/m. A small leak into the cavity vacuum manifested itself when the cryostat was cooled down; the pressure in the cavity was about 10^{-6} torr at 2 K.

5.2 Follow-Up Tests on the First Cavity

The failed RF cable was replaced, the vacuum leak was fixed, and the cavity was retested 1 week after the first RF test (without exposure of the inside of the cavity to air). A gradient of about 7 MV/m was reached. It was thought that helium processing might be beneficial, but the test had to be stopped early due to scheduled maintenance of the cavity testing facility.

The next opportunity for an RF test was in January 2003. In between tests, the cavity was etched to remove another 50 μm from the inner surface and the high-pressure water rinsing was repeated. The final filter on the high-pressure rinsing system (between the pump and the nozzle) was temporarily unavailable at the time of this rinse.

The results of the January 2003 test are also shown in Figure 7 (circles). The low-field Q_0 was smaller than in the first test, although the difference is within the margin of reproducibility of the measurement. A gradient of about 11 MV/m was reached. The decrease in Q_0 between 9 and 11 MV/m is likely due to field emission; the x-ray signals were larger (> 1.5 rem/hour) than those seen in the first RF test. Thus the difference between the September 2002 and January 2003 tests could be due to particulate contamination during the high-pressure rinse without the final filter. Although the field level was not as high as in the first test, Q_0 was nevertheless in excess of 10^{10} at $E_a = 8$ MV/m.

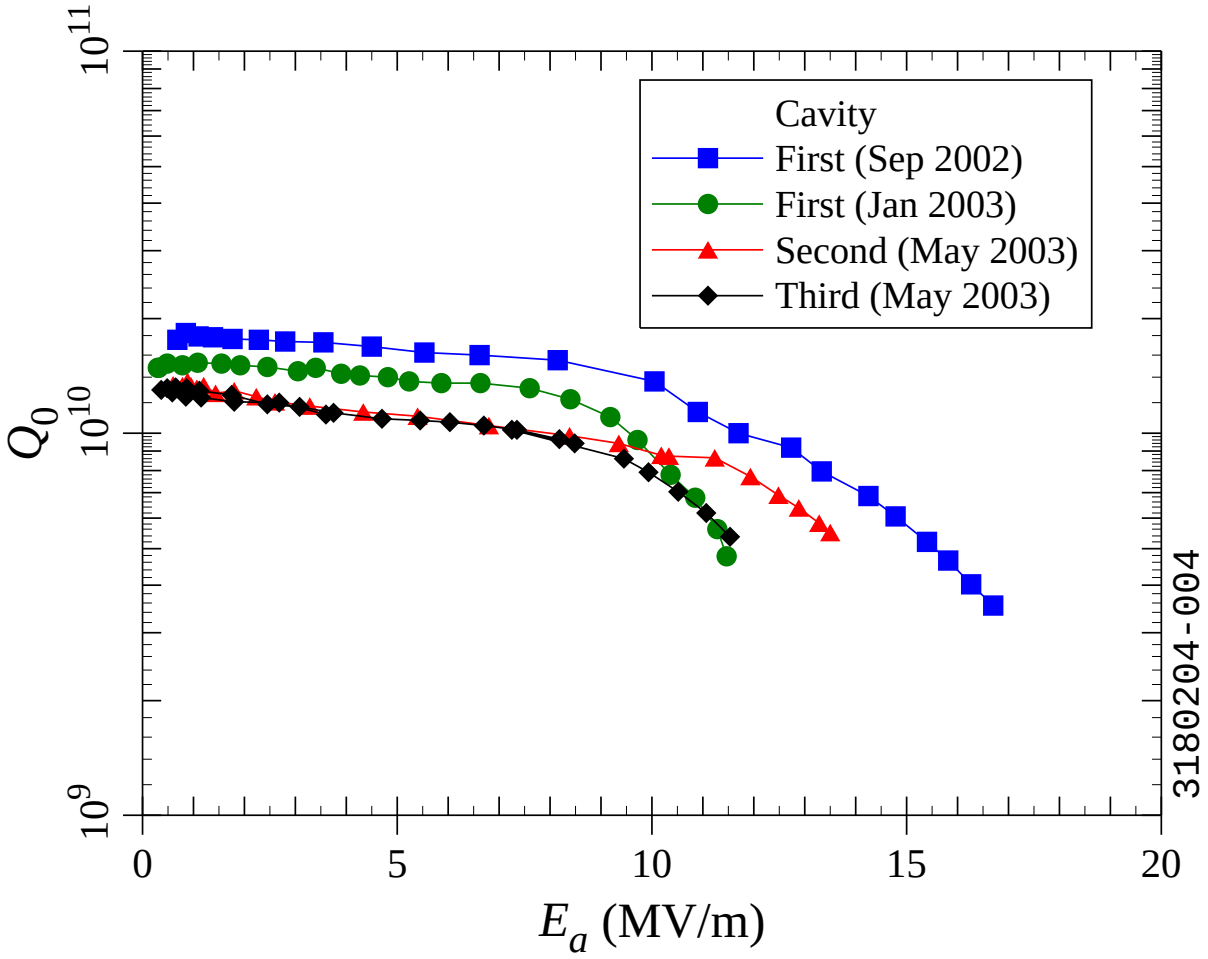

Figure 7. Measured dependence of the quality factor on the accelerating gradient for the 6-cell cavity prototypes. All measurements were done at a bath temperature of 2 K.

5.3 Tests on the Second Cavity

The second cavity was tested in May 2003. In the first RF test, a gradient of 8 MV/m was reached at 2 K. The Q_0 was lower ($8 \cdot 10^9$) and some Q-switching was seen, indicating that more etching was needed.

In preparation for a second RF test, another 150 μm was removed from the inner surface, and the high-pressure rinse was repeated. Results from the second test are shown in Figure 7 (triangles). A gradient of 13 MV/m was reached. The Q_0 was 10^{10} at $E_a = 8$ MV/m. The field was limited by the available RF power (the input coupling was weaker than planned). The x-ray signals were small (10 mrem/hour maximum).

5.4 Tests on the Third Cavity

The third cavity was also tested in May 2003. Results are shown in Figure 7 (diamonds). A gradient of 11 MV/m was reached. The Q_0 was again about 10^{10} at $E_a = 8$ MV/m. The field was again limited by the available RF power (the same weak input antenna was used). As with the second cavity, the x-ray signals were small (0.5 mrem/hour maximum).

5.5 Temperature Dependence

Small RF losses in the cavity are desirable to minimise the load to the cryogenic system. Low RF losses correspond to a large Q_0, or, equivalently, a small RF surface resistance R_s, since $Q_0 = G/R_s$, where G is the geometry factor. An approximate expression for the surface resistance of Nb is [29]

$$R_s(T) = R_0 + C_{RRR} R_1 \frac{T_\Delta}{T} \left(\frac{f}{f_1}\right)^2 \exp\left(-\frac{T_\Delta}{T}\right) , \qquad (1)$$

where T is the temperature, f is the RF frequency, $T_\Delta = 17.67$ K, $R_1 \cdot T_\Delta = 2 \cdot 10^{-4}\ \Omega \cdot$ K, and $f_1 = 1.5$ GHz; R_0 is the temperature-independent residual surface resistance. The coefficient C_{RRR} is 1 for reactor grade Nb (RRR = 25) and about 1.5 for high purity Nb with RRR = 250. As the surface purity can be different from the bulk purity, C_{RRR} can be considered to be a fitting parameter. Equation (1) is valid for $f \ll 1$ THz and $T \leq 4.6$ K.

Figure 8 shows the measured RF surface resistance at low field ($E_a \leq 0.8$ MV/m) as a function of $1/T$. The solid lines are calculated from Equation (1), assuming $C_{RRR} = 1.25$ and the indicated R_0 values. In all cases, the surface resistance at higher temperatures follows Equation (1) reasonably well. This suggests that the surface RRR is smaller than the nominal bulk value of 250, but higher than that of reactor grade Nb. The R_s values at low temperatures are consistent with R_0 being between 2 and 9 nΩ.

The results for the single-cell cavities were similar to those of the 6-cell cavities. In the best single-cell tests, the temperature-dependent losses were slightly lower than for the 6-cell cavities.

In the January 2003 test on the first 6-cell cavity, measurements of Q_0 as a function of gradient were done at several different temperatures, as shown in Figure 9. A significant downward slope in Q_0 can be seen for the measurements above the superfluid transition temperature (2.15 K), as is typically seen. Thus, high-field operation of the cavities is more economical for $T < 2.15$ K, as one would expect. The low-field Q_0 at 1.8 K is significantly higher than at 2 K, which confirms that the temperature-dependent losses are still contributing to the surface resistance. However, the maximum gradient at 1.8 K is only slightly higher (11.4 MV/m) than at 2 K.

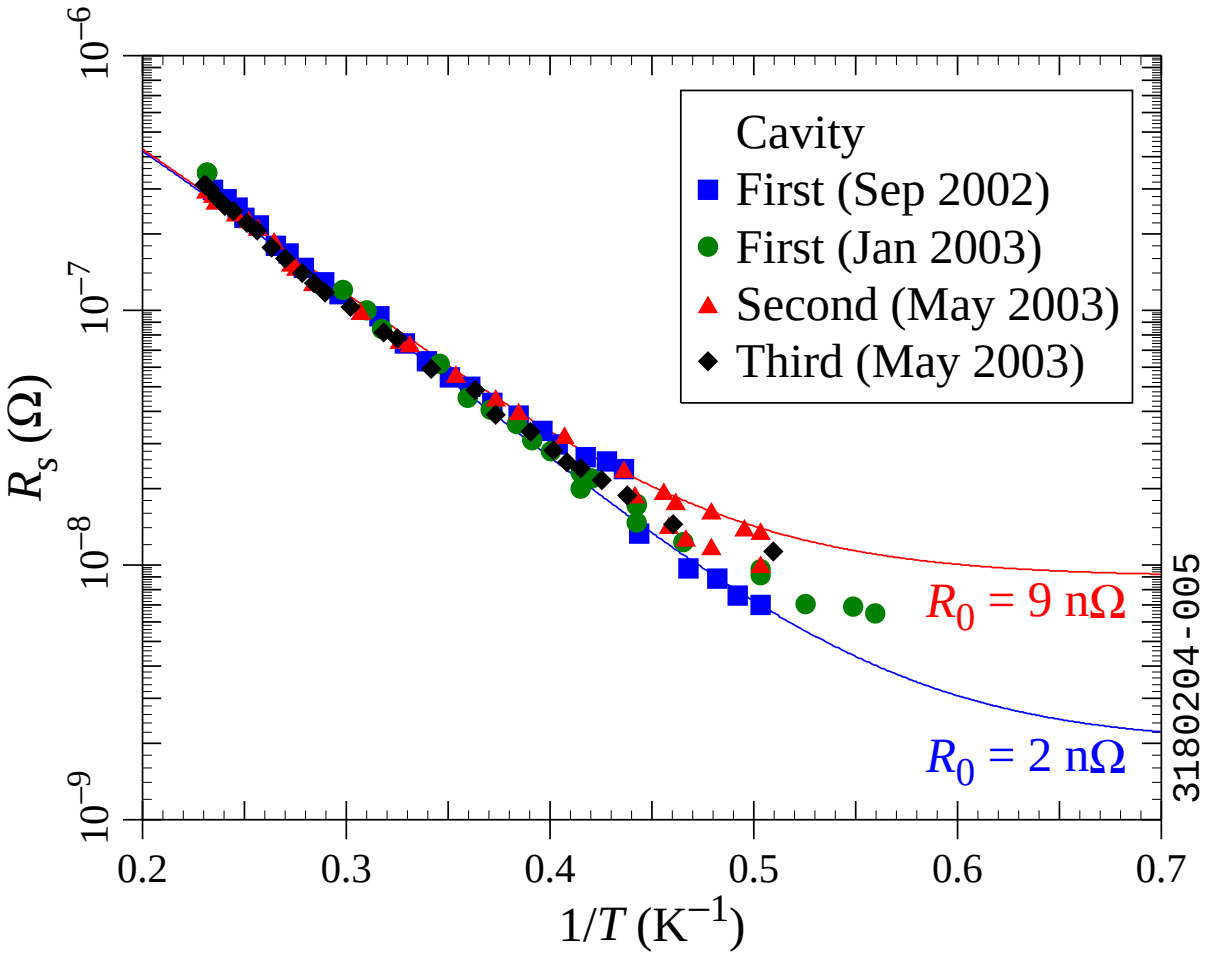

Figure 8. Measured dependence of the RF surface resistance on bath temperature for the 6-cell cavity prototypes. The solid lines are theoretical predictions for $C_{RRR} = 1.25$ and $R_0 = 2$ or 9 nΩ.

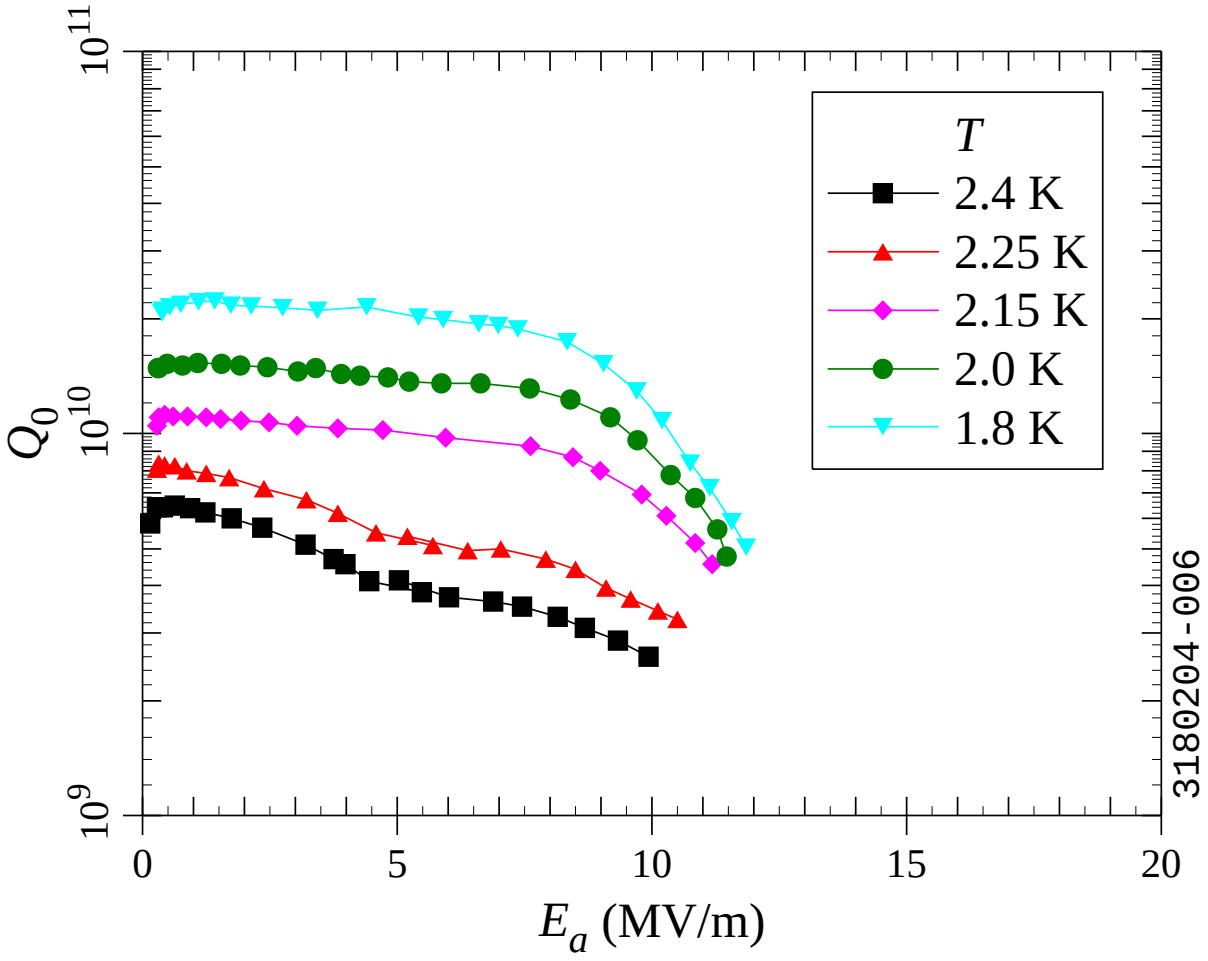

Figure 9. Measured dependence of the quality factor on the accelerating gradient at different bath temperatures for the first 6-cell cavity prototype (January 2003).

6 Cryomodule Design and Fabrication

Beam dynamics simulations for efficient beam transport with minimal emittance growth have shown that four $\beta = 0.47$ cavities per cryomodule with cavity alignment tolerances of ± 1 to 2 mm are acceptable [30]. Figure 10 shows the production cryomodule with four 805 MHz $\beta = 0.47$ six-cell cavities. Figure 11 shows the prototype cryomodule with two cavities. Table 2 gives the main parameters for both the production cryomodule and the prototype cryomodule.

Figure 12 shows a cavity with its helium vessel made of titanium, its RF input coupler, and its tuner. The Ti vessel is TIG welded to Nb-Ti adapter flanges that are electron beam welded to the Nb cavity beam tubes. The first transverse mechanical mode of the cavity is damped by attaching the center of the cavity to the helium vessel with three titanium spokes; the design is a simplified version of the "spider" support used for the SNS vessels. A titanium to stainless steel transition is used to attach the cavity to the helium manifold. No higher order-mode dampers are required due to the relatively low beam current [27].

Table 2. Design parameters for prototype and production cryomodules.

Item	Prototype	Production
Cavities	2	4
Length	2.1 m	4.0 m
2 K cold mass	210 kg	460 kg
Total mass	2200 kg	3600 kg
Bayonets	2	4
Support links	4	4
77 K heat load	< 50 W	< 100 W
2 K Heat Load		
Input coupler	1.6 W (each)	
Tuner	0.8 W (each)	
Total (RF off)	9 W	15 W
Total (RF on)	53 W	103 W

6.1 Input Coupler

The coupler parameters are summarised in Table 3. The required RF power for beam loading and microphonics control is less than 10 kW [15]. The ceramic window is the same as that used for the SNS couplers [31, 32]. A smaller diameter is used in the vacuum coaxial line for capacitive coupling to the cavity [33]. The outer conductor does not require helium gas cooling, which simplifies the cryogenic distribution system. The thermal load from the

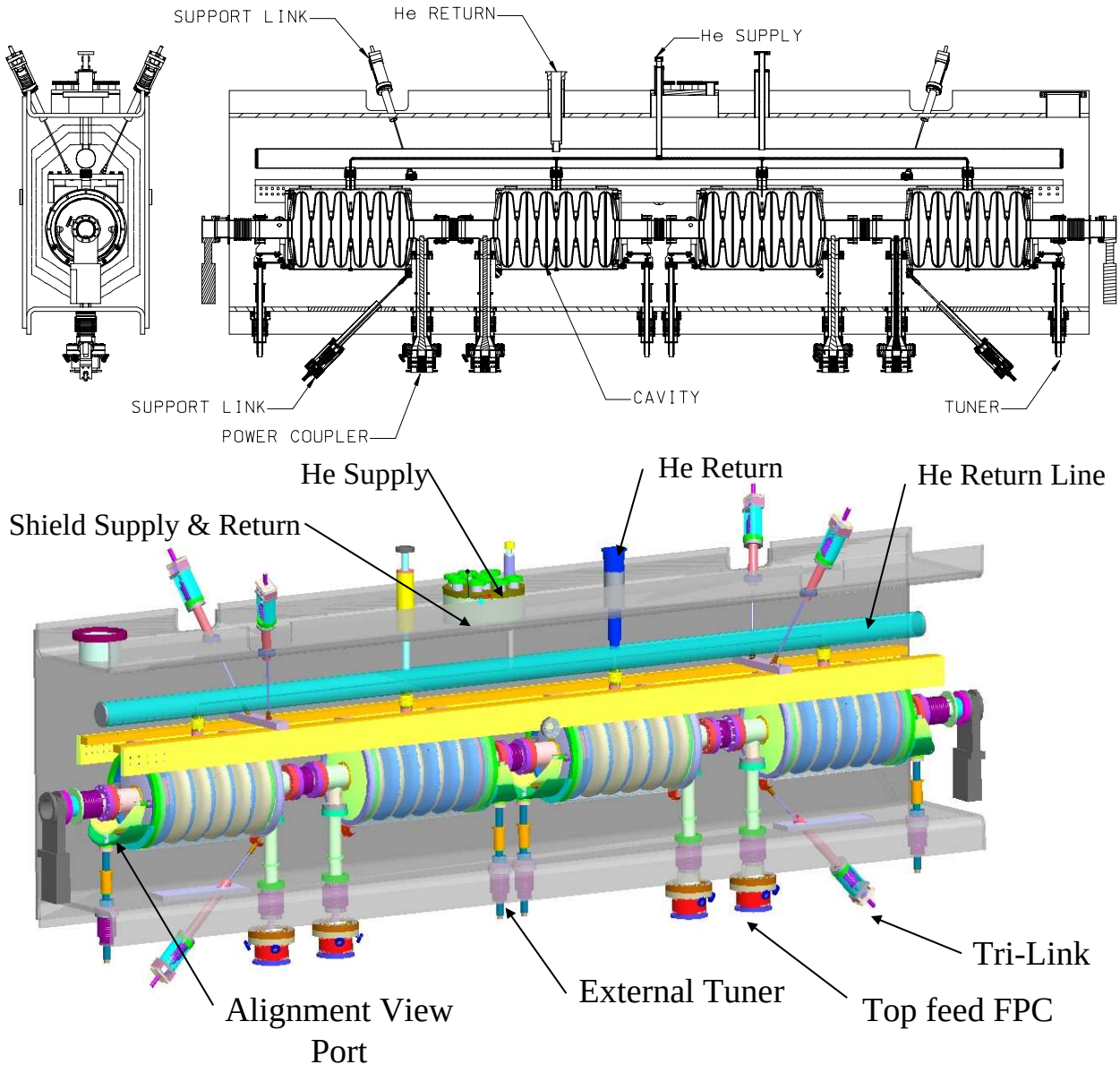

Figure 10. Drawings of the production cryomodule: end view, side view, and isometric view.

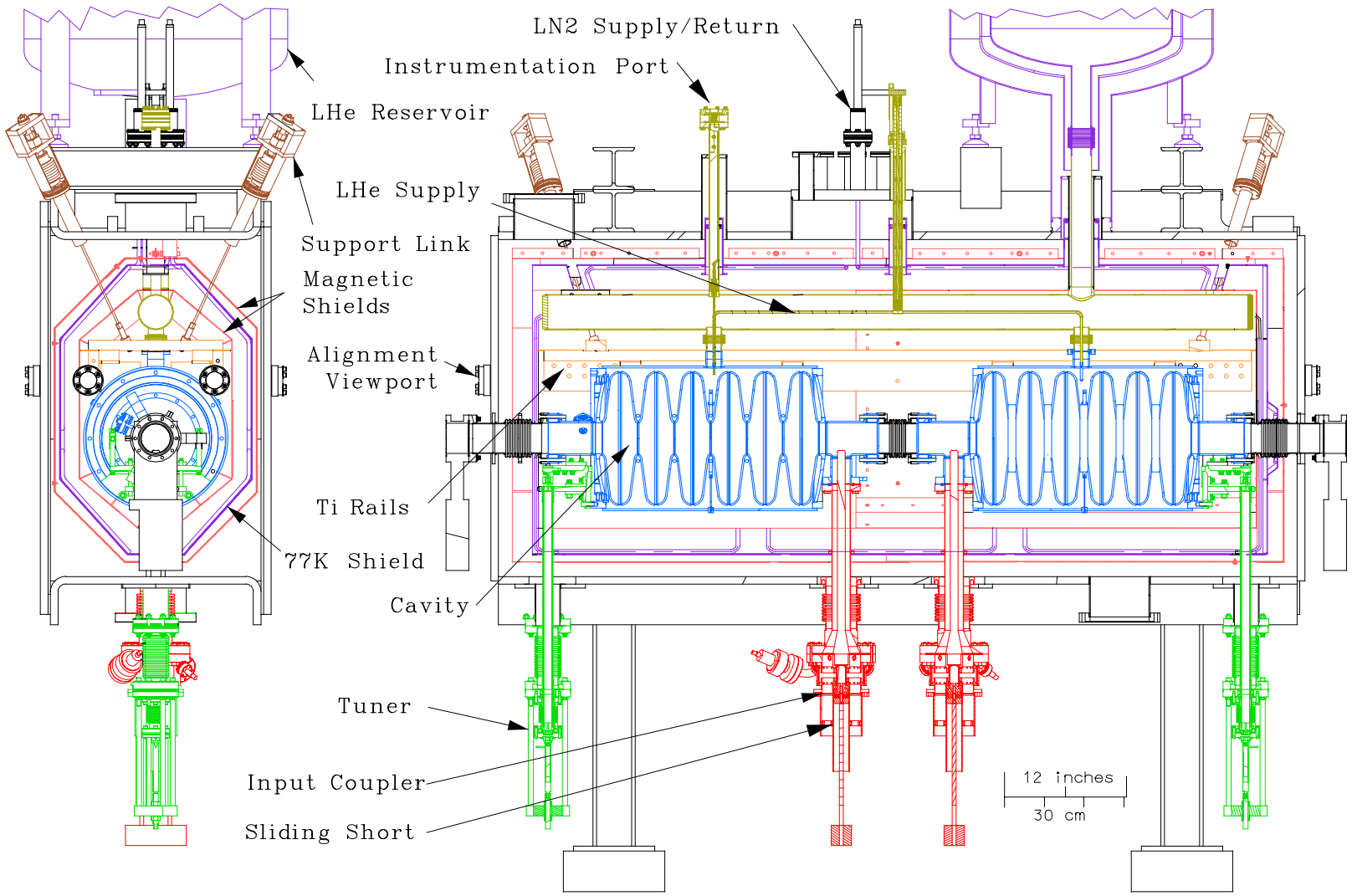

Figure 11. Drawings of the prototype cryomodule: end view and side view.

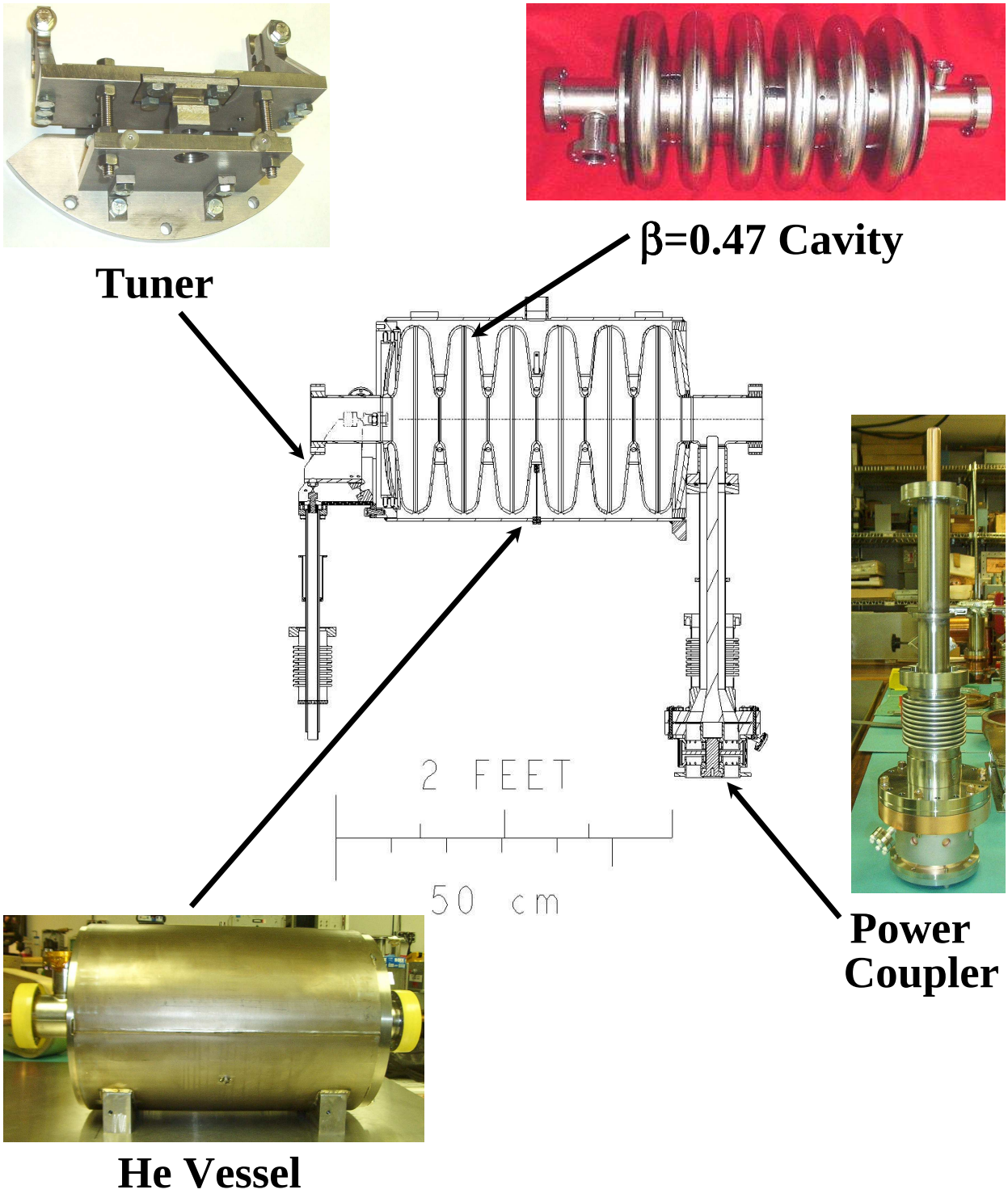

Figure 12. Components associated with each cavity in the prototype cryomodule.

Table 3. RF input coupler parameters.

Impedance	50 Ω
Type	Planar Coax (KEK/SNS)
Cooling	conduction
Q_{ext}	$2 \cdot 10^7$
Bandwidth	40 Hz
Design power	5 kW
Max power	100 kW

power coupler to the helium system was calculated assuming 10 kW of RF power and a center conductor at room temperature. The outer conductor is 0.89 mm thick stainless steel with 8 μm of copper. Figure 13 shows the temperature profile along the outer conductor, which has a liquid nitrogen intercept. Note that the distribution shown in Figure 13 is slightly different from the preliminary distribution presented previously [21]. The helium and nitrogen load are 1.6 and 4 W per coupler respectively. Operation with 50 K helium gas in lieu of liquid nitrogen would further decrease the helium load.

The couplers were conditioned prior to installation onto the cavities, following procedures similar to those used for the SNS couplers [34].

6.2 Tuner

As shown in Figure 14, the tuner was designed to be actuated from outside the cryomodule. External actuation allows for easier maintenance, since it is not necessary to warm up the cryomodule and vent the insulation space in order to access the actuator. Tuning is done by shortening or lengthening the cavity. The force is transmitted from below via two concentric tubes and a rocker mechanism. The rocker mechanism transmits the force to the beam tube of the cavity; it is anchored to the helium vessel. Bellows are included in the helium vessel between the outer cylinder and the end dish to reduce the tuning force.

Actuation can be done with a stepping motor for slow (coarse) tuning and a piezo-electric actuator for fast (fine) tuning. The piezo actuator can be used to damp microphonics if needed. Since the cavities will operate in continuous wave (CW), Lorentz detuning will not require fast compensation.

6.3 Suspension and Alignment

All four cavities are rigidly aligned on a titanium rail with optical fiducials at the ends and center of the rail that can be viewed when cooled to 2 K to verify alignment. The 2 K cold mass is assembled in a clean room. The cavities are aligned using push-pull mechanisms and shims outside the clean room. The 2 K cold mass is supported with six nitronic links. The

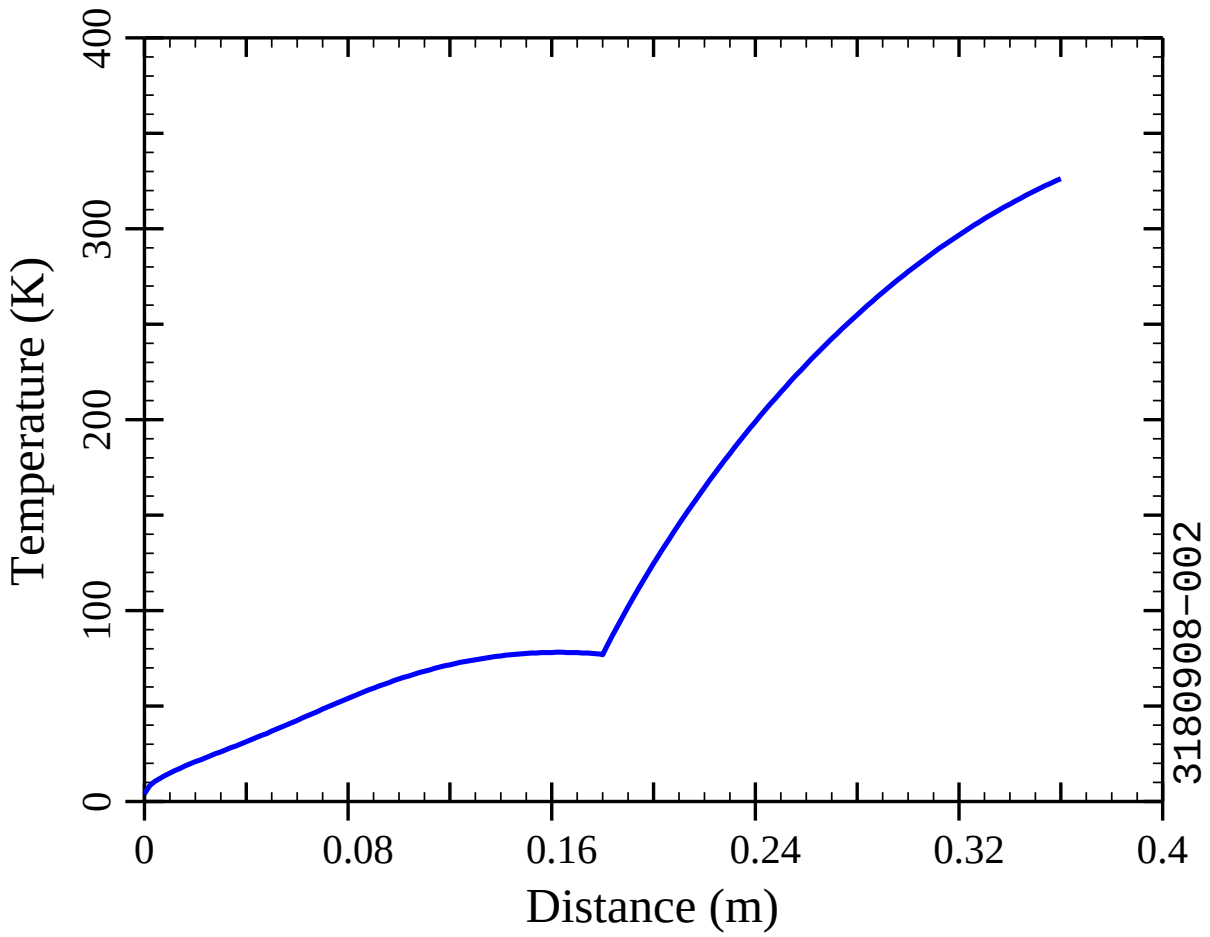

Figure 13. Calculated temperature distribution along the outer conductor of the RF coupler.

link forces are monitored using strain gauges. The two magnetic shields and the 77 K thermal shield are supported by the helium distribution plumbing and are hence mechanically isolated from the 2 K cold mass. The vacuum vessel is made from low carbon steel plate. During transportation, pins secure the cold mass to the vacuum vessel, and a stiffener is inserted into the power coupler. The component most sensitive to shock is the power coupler's inner conductor, which will plastically deform above 4.6g.

6.4 Shields and Cryogenic Distribution

The two μ-metal shields reduce the stray magnetostatic fields to between 0.5 and 1 μT. The μ-metal shields also serve as passive thermal shields. Liquid N_2 was used in the thermal shield for the prototype cryomodule, but, in the production cryomodules, 50 K He gas

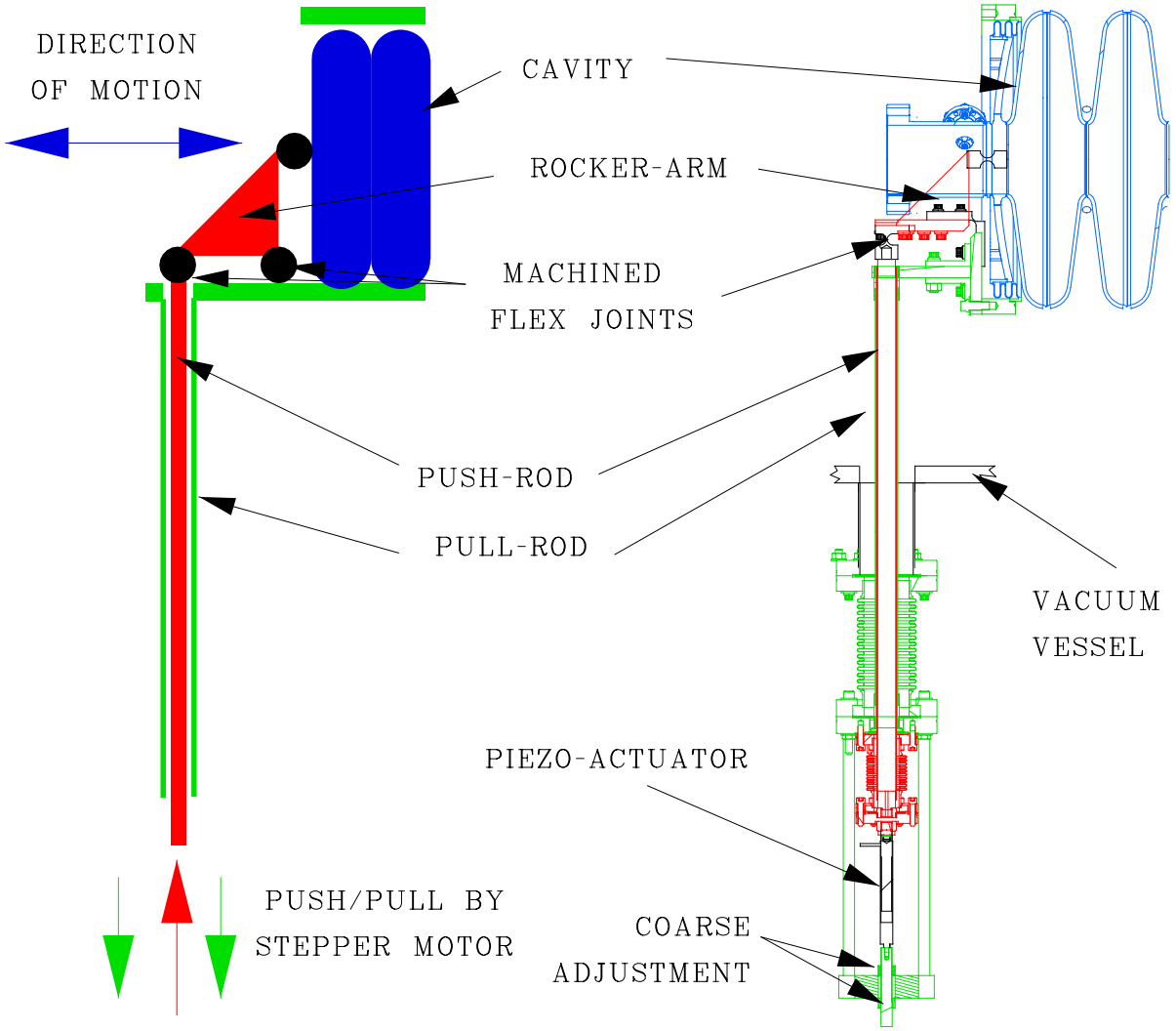

Figure 14. Left: schematic representation of the tuner and tuning forces. Right: drawing of the tuner attached to the cavity.

will be used, which will further decrease the static load to the liquid He. In the prototype cryomodule, a helium reservoir was used on top of the cryomodule. In the production cryomodule, the cryogenic distribution system will house the control valves and heat exchangers to simplify the cryomodule and allow commissioning of the cryogenics before installation of the cryomodule.

6.5 Design Features

The rectangular cryomodule with titanium rails offers several advantages over that used for SNS. The rectangular design concept can be used for quarter-wave and half-wave cavities,

in addition to elliptical cavities, allowing for an entire linac with the same basic cryomodule design throughout. It is anticipated that the rectangular cryomodule could cost less than half that of the SNS cryomodules. The smaller helium vessel simplifies the preparation steps for the cavities and decreases the cryomodule width, thereby allowing for a smaller tunnel width. Also, the titanium rail and small helium vessel simplify fixturing and alignment of the cavities. The lower power RF couplers do not require helium gas cooling, which simplifies the coupler design and cryogenics. With the cryogenic controls adjacent to the module, the room temperature slot length for diagnostics and focusing elements can be reduced, allowing for a decrease in the tunnel length. The cavity tuner is actuated at room temperature, that maintenance on the actuator can be done without having to warm up the cryomodule and vent the insulation vacuum.

6.6 Prototype Cryomodule Fabrication

The cold mass, including cavities, helium vessels, input couplers, and beam line, was assembled at Jefferson Laboratory in a class 10 clean room and shipped by truck to MSU. The cavities were shipped under partial vacuum due to a leak in a valve, which was subsequently replaced.

The cryomodule was assembled around the cold mass. Figure 15 shows photographs taken at various steps in the cryomodule assembly sequence. A simple fixture was used to verify cavity alignment to the beam axis within ± 0.25 mm. Fiducials on the Ti rails were monitored through viewports during the cool-down.

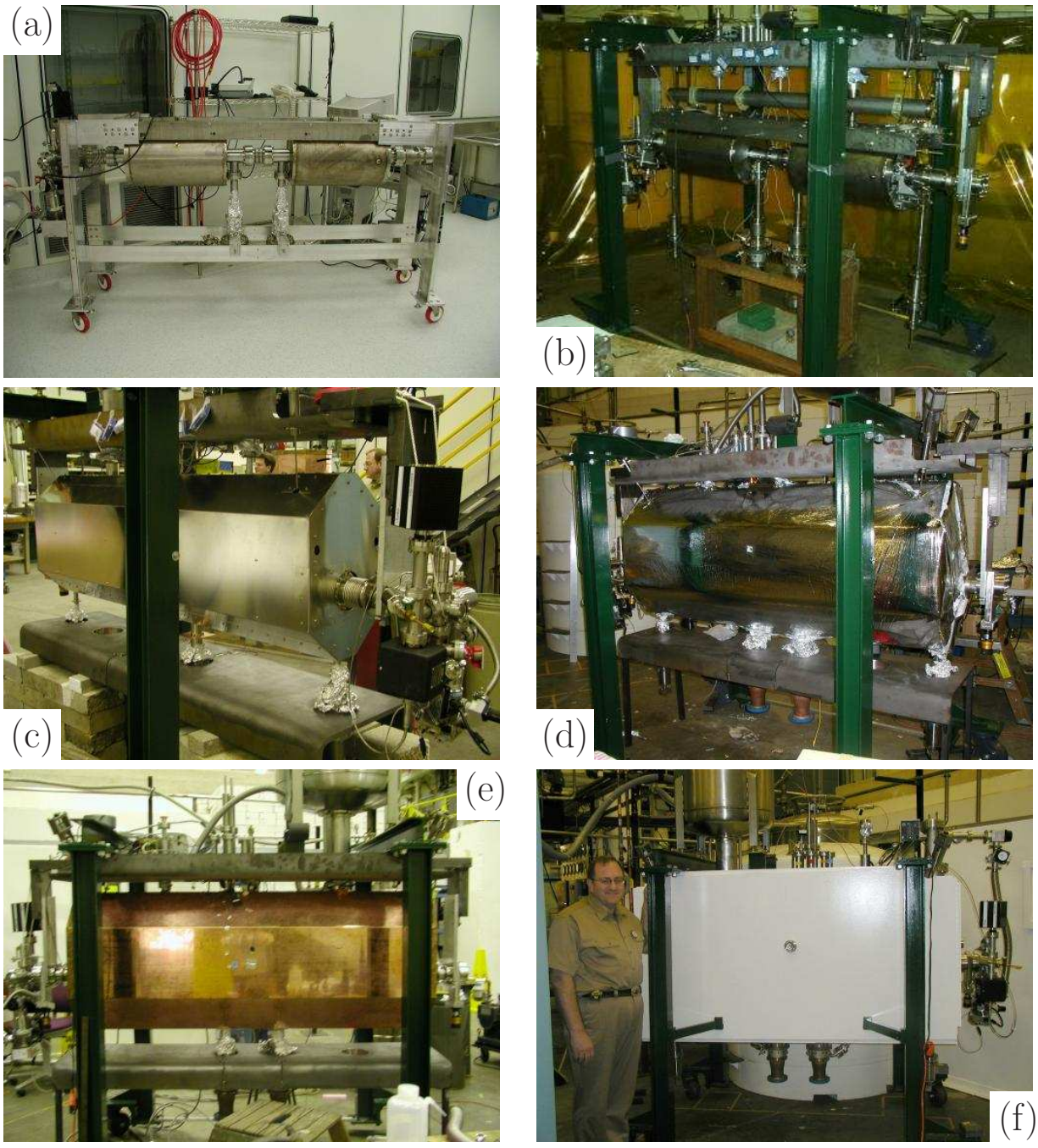

Figure 15. Fabrication of the prototype cryomodule: (a) cold mass, including cavities, helium vessels, Ti rails, and input couplers; (b) cold mass suspended from top plate; (c) inner μ-metal shield and bottom plate; (d) multi-layer insulation; (e) 77 K thermal shield and helium reservoir; (f) completed cryomodule.

7 Testing of the Prototype Cryomodule

Testing of the prototype cryomodule was done at MSU, with the cryogens supplied by the NSCL cryogenic plant.

7.1 Cool-Down

The cool-down to 20 K was done rapidly to avoid Q disease. Below 20 K, we proceeded slowly to economise liquid He while the cryomodule approached steady state. The cavities reached 24 K in about 2.5 hours and became superconducting after another 2.5 hours. He gas was introduced into the insulation vacuum space for about 3 hours during the cool-down to increase the heat transfer to the liquid N_2 shield. The cryomodule temperatures were nearly at their steady state values with a full He reservoir 16 hours after the cool-down started. The cavities were cooled from 4.3 K to 2 K by pumping on the He reservoir.

In the initial attempt to cool down to 4 K, the insulation vacuum was not spoiled and the He reservoir was filled rapidly—this caused problems due to the inner μ-metal shield and Ti rails still being warm. In the production cryomodules, it may be worthwhile to improve the heat sinking for these elements to simplify the cool-down.

In initial attempts to cool down to 2 K, there were 2 trapped gas volumes in the liquid He space, one in the supply bayonet and the other associated with a viewport on top of the module. These trapped gas volumes produced thermo-acoustic oscillations near the λ-point, resulting in a pressure instability. Once the liquid level was low enough so that the gas was no longer trapped, we were able to reach 2 K. This problem was eliminated by removing the supply bayonet and the viewport and plugging the holes with teflon-tipped G10 spears. (A supply bayonet was installed in the He reservoir to replace the original bayonet feeding liquid directly to the cavities.) Trapped gas volumes will be avoided in the production cryomodules.

7.2 Static Heat Leak

The static heat leak to the liquid He at 2 K was measured from the volume of He gas pumped per unit time. The pumping rate was obtained by measuring the time required to displace a known volume of water. The pumping rate was converted to heat leakage rate by calibrating it against a resistive heater in the cryomodule. In steady state conditions, the measured static heat leak to the liquid He was 10 to 11 W. As was indicated in Table 2, the predicted heat leak is 9 W for the prototype cryomodule, which is in reasonable agreement with the measured value. It should be noted that the measured static heat leak includes heat leakage into the liquid helium reservoir on top of the cryomodule, but the predicted static heat leak does not take into account the reservoir.

The static heat leak to the liquid He at 4.3 K was measured from the rate of decrease of the level in the He reservoir. As expected, the measured heat leak at 4.3 K (9 W) was similar to that at 2 K.

7.3 Input Couplers

The measured input coupling strengths were $Q_{ext} = 1.4{\cdot}10^7$ for Cavity #1 and $Q_{ext} = 1.3{\cdot}10^7$ for Cavity #2, both a bit lower than the design value ($Q_{ext} = 2 \cdot 10^7$).

Multipacting barriers were encountered at low field ($E_a \lesssim 0.1$ MV/m) with both cavities after they were cooled to 4.2 K. In both cases, we punched through the barriers after less than 1 hour of RF conditioning. Current was detected on the center conductor during the conditioning, which suggests that the multipacting was in the coupler, not in the cavity.

Since the input antennae cannot be moved, sliding shorts were installed on the coaxial lines to adjust the input coupling (see Figure 11). Loop antennae on the sliding shorts were used to couple power in and excite a standing wave in the coupler. For high field measurements, the short was moved to the detuned position to maximise the field in the cavity and minimise the field in the coupler. For low-field microphonics studies with a wide band-width, the short was moved to the tuned position. The range of measured Q_{ext} values was $6 \cdot 10^4$ to $6 \cdot 10^9$.

7.4 Cavities

The sliding short allowed us to set up a good match to reach high fields without high RF power, so most of the RF measurements were done with a 200 W solid state amplifier and a phase feedback loop.

The intrinsic quality factor of the cavity (Q_0) was obtained from RF measurements and checked with calorimetry. With the short present, the coaxial line has one open end and one shorted end, and hence has resonances when the length is equal to an odd integer multiple of $\lambda/4$. In the detuned position, the cavity resonance was between the frequencies of the $7\lambda/4$ and the $9\lambda/4$ resonances. We measured the Q for these adjacent resonances to estimate the power dissipation in the coupler's standing wave. We used a second loop antenna to infer the energy stored in the standing wave while we were driving the cavity. This allowed us to subtract out the estimated power dissipation in the coaxial line and calculate Q_0 directly from the RF measurements.

Field emission started at low field in the first measurements at 2 K. The field emission was especially bad in Cavity #1. Interesting images were observed with a video camera (set up to look into the cavities from a viewport on the beam tube) while driving Cavity #1. The light disappeared during RF processing of Cavity #1 and did not return. We were able to reach $E_a = 6$ MV/m in Cavity #1 and $E_a = 7.5$ MV/m in Cavity #2 after RF processing. We observed some deconditioning of Cavity #2 after conditioning of Cavity #1.

Additional pulsed processing (power ≤ 3 kW) was done to further reduce the field emission. Figure 16 shows the cavities' performance after pulsed processing. The design gradient ($E_a = 10$ MV/m) was exceeded in both cavities, but they both still showed field emission at high field: after processing, the first x-ray signals were detected at $E_a \approx 8$ MV/m, and the x-ray levels near the cryomodule reached as high as 10 rem/hour at high field. Cavity #2 does not quite meet the design goal of $Q_0 = 7{\cdot}10^9$ at the design gradient. After conditioning, both cavities exhibited some "Jekyll & Hyde" behaviour in which the field emission current

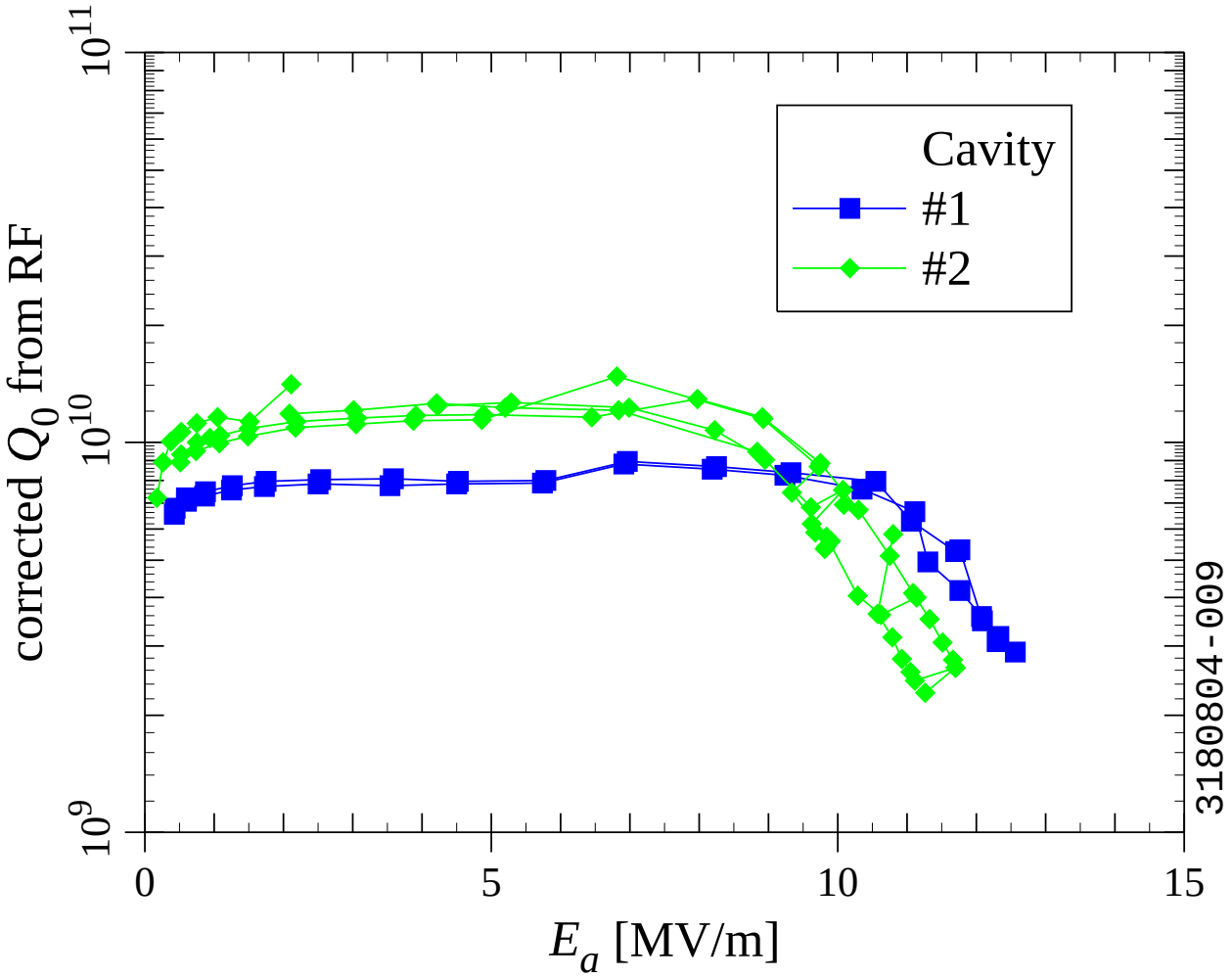

Figure 16. RF measurements on the $\beta_g = 0.47$ cavities at 2 K after RF processing.

(along with the RF power dissipation and x-ray flux) jumped back and forth between a lower value and a higher value. This can be seen most clearly from the double-valued Q_0 versus E_a curve for Cavity #2 at high field.

Measurements on the standing wave indicated that, at low field, the power dissipation in the coaxial line was less than or about equal to the power dissipation in the cavity; at high field, a higher proportion of the power was dissipated in the cavity. To check the RF measurements, the quality factor was obtained from a calorimetric measurement of the power dissipation. As for the static heat leak measurement, the He gas pumping rate was measured and calibrated against a heater. Measurements were done on Cavity #2 before the final round of pulsed RF processing. Useful results were obtained for $4.5 \leq E_a \leq 7$ MV/m (at low field, the RF power dissipation was small relative to the static heat leak and the uncertainty in Q_0 was excessive). The calorimetric Q_0 values were between $5 \cdot 10^9$ and $9 \cdot 10^9$,

consistent with the RF measurements.

7.5 Tuners

The tuner results are summarised in Table 4. In the first cool-down to 2 K (both tuners locked), the resonant frequencies were 805.13 MHz (Cavity #1) and 805.24 MHz (Cavity #2). Figure 17a shows the measured frequency shift as a function of actuator displacement. The measured travel of the tuner actuator was 10 mm, with a measured tuning range of about 1 MHz. Thus, the measured tuning range was greater than the design goal of 0.5 MHz by a comfortable margin, and both cavities were well within tuning range of the design frequency of 805 MHz. A piezo-electric actuator was installed for fast tuning and compensation of vibrations. Figure 17b shows the measured frequency shift as a function of drive voltage to the piezo actuator. The range of fast tuning with up to 100 V drive signal was about 11 kHz. There is some hysteresis, as can be expected for piezo-electric actuators. The piezo actuator was used for active damping of microphonics [15, 16].

Table 4. Summary of tuner measurements and comparison with design goals.

Item	Design	Measured
Range	$\pm$250 kHz	$\pm$500 kHz
Tuning coefficient	$>$ 200 kHz/mm	208 kHz/mm
Cavity spring constant	$<$ 1750 N/mm	1910 N/mm
Resolution	1 Hz	
Compliance	0.7 (rigid)	0.5

8 Multipacting

The RF tests on single-cell cavities showed that there are no hard multipacting barriers. A soft multipacting barrier was seen occasionally at very low field ($E_a < 1$ MV/m). After we introduced gas for He processing, the barrier became more persistent, but we could still punch through it. Multipacting simulations [23, 35] also indicate that there should be no hard barriers in the single-cell cavities.

No multipacting problems were encountered in the vertical RF tests on the multi-cell cavities. As discussed in Section 7.3, soft multipacting barriers were observed at low field during the horizontal tests on the cavities, but were likely associated with the couplers rather than the cavities.

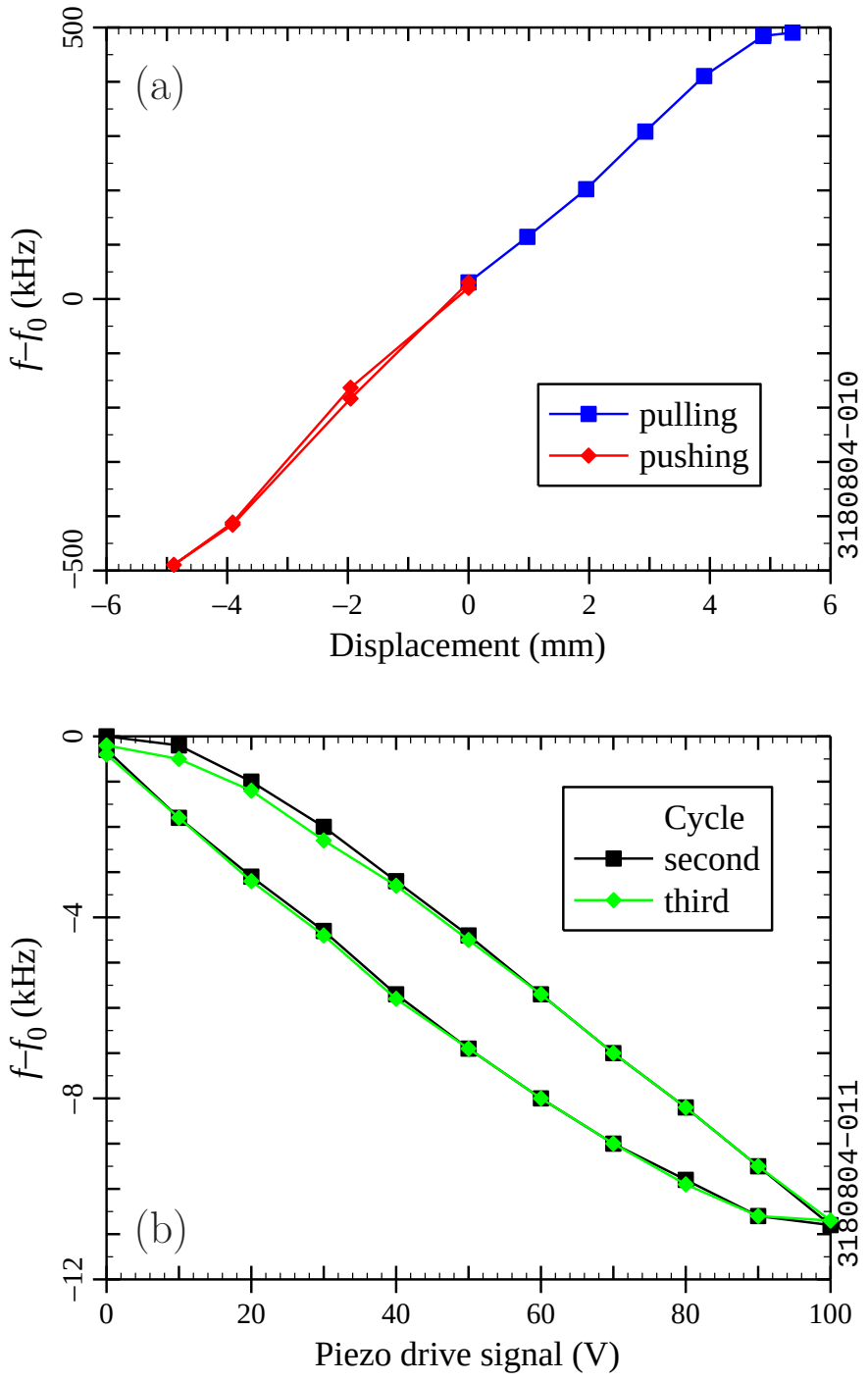

Figure 17. Measurements of (a) coarse tuning and (b) fine tuning of the cavity; f_0 is the starting frequency.

9 Frequency Issues

When a cavity is used for acceleration of a beam, the resonant frequency of the cavity must be close enough to the design frequency to maintain the desired amplitude and phase. Disturbances which can shift the resonant frequency include fluctuations in the pressure of the helium bath, Lorentz detuning due to the electromagnetic field in the cavity, and mechanical vibrations (microphonics). Measurements were done on the cavities to quantify these effects.

The rate of change in the resonant frequency f as a function of the pressure P in the helium bath was measured during the cool-down from 4.2 K to 2 K in the single-cell tests, multi-cell vertical tests, and multi-cell horizontal tests. For the 6-cell cavities installed in the prototype cryomodule, the measured values were $df/dP = 0.36$ kHz/torr (Cavity #1) and $df/dP = 0.46$ kHz/torr (Cavity #2). The sign is the opposite of what was measured for single-cell cavities ($df/dP = -1.0$ kHz/torr) and vertical tests on 6-cell cavities; the pressure force on the helium vessel (present for the cryomodule cavities, absent in the vertical tests) tends to cancel the effect of the pressure force on the cavities.

Lorentz force detuning was also measured for the single-cell and multi-cell cavities. For the 6-cell cavities in the prototype cryomodule, the measured Lorentz detuning coefficient at 2 K was $K_L \equiv df/dE_a^2 = -16$ Hz/(MV/m)^2. This result is close to the predicted value of $K_L = -14$ Hz/(MV/m)^2 [23]. The value measured in the cryomodule is smaller than the measured detuning for the single-cell cavities [$K_L = -22$ Hz/(MV/m)^2], as one would expect since the single-cell cavities had no stiffening rings at the irises.

Microphonics are not very serious for SNS due to the high beam current, which requires large cavity bandwidths. A 400 kW heavy ion linac would have significantly lower beam current, so microphonics issues are more serious. The stiffening rings of the SNS cavities are included in the $\beta_g = 0.47$ cavity to reduce microphonic excitation (see Figure 5 above). As mentioned previously, lateral bracing similar to the center support "spider" of the SNS cavities [11, 36] is also implemented. The $\beta_g = 0.47$ cavity is overcoupled to ensure that the gradient can be maintained in the presence of microphonics [27]. Some microphonic measurements were done on a single-cell cavity [18]. In the prototype cryomodule test, the piezo-electric actuator was used for active damping of microphonics. Sinusoidal disturbances were controlled using adaptive feed-forward cancellation. The results are reported in separate papers [15, 16]. Control of the RF amplitude and phase was also demonstrated. The RF control studies are described in a separate report [37].

10 Conclusion

A research and development program for six-cell $\beta_g = 0.47$ superconducting cavities has been carried out. The first step was prototyping of single-cell and six-cell cavities. RF tests were done on two single-cell $\beta_g = 0.47$ cavity prototypes and three 6-cell cavities with encouraging results: all of the cavities exceeded the goal of 10 MV/m accelerating gradient, with $Q_0 \geq 7 \cdot 10^9$ at $E_a = 10$ MV/m and $Q_0 \geq 10^{10}$ at $E_a = 8$ MV/m. The first 6-cell cavity

and both single-cell cavities reached $E_a \geq 16$ MV/m; the second and third 6-cell reached 13 MV/m and 11 MV/m, respectively. The three niobium multi-cells and one copper multi-cell were tuned for field flatness.

The second step was the design and fabrication of a prototype cryomodule, followed by horizontal testing of two of the six-cell $\beta_g = 0.47$ cavities in the module. A rectangular box cryomodule was used. The desired cryogenic and RF performance of the system was demonstrated. The RF performance of one of the cavities is a bit marginal due to contamination. It should be noted that SNS production cavities were prepared using the same facilities at about the same time (November 2003), and they showed similar problems with field emission. Corrections have since been implemented, resulting in lower field emission and better performance for SNS cavities. A valve leak might have also contributed to the contamination of the prototype module.

The results suggest that one should be able to achieve performances with $\beta_g = 0.47$ cavities similar to those of other $\beta < 1$ elliptical cavities, and that a rectangular cryomodule should be suitable for a heavy ion linear accelerator. One can anticipate that that high-field performance of $\beta_g = 0.47$ cavities will be strongly correlated with the degree to which particulate contamination can be controlled, as has been observed for other superconducting cavities.

11 Acknowledgments

We thank the staff at INFN Milano, Jefferson Lab, and MSU for their hard work in the design, fabrication, preparation, and testing the cavity prototypes. R. Afanador, J. Brawley, B. Manus, S. Manning, S. Morgan, and G. Slack provided essential support with the fabrication and chemical treatment of the cavities at Jefferson Lab. A. Aizaz, J. Bierwagen, J. Brandon, D. Capelli, J. Colthorp, S. Hitchcock, H. Laumer, D. Lawton, A. McCartney, D. Pedtke, L. Saxton, J. Vincent, and R. Zink provided valuable support at NSCL.

The design, fabrication, assembly, and testing of the prototype cryomodule benefited from the help of many people. Collaborators from outside NSCL include T. Kandil, H. Khalil, L. Kempel, A. Moblo, M. O'Farrell, C. Radcliffe, M. Stirbet, and C. Wiess.

W. Schneider reviewed the cryomodule design and provided valuable feedback. The RF input couplers were fabricated by AMAC International.

This work was supported by the U.S. Department of Energy under Grant DE-FG02-03ER41247.

References

[1] Henry A. Thiessen, "PILAC: A Pion Linac Facility for l-GeV Pion Physics at LAMPF," in *Conference Record of the 1991 IEEE Particle Accelerator Conference, San Francisco, CA*, Loretta Lizama and Joe Chew, Editors, IEEE, Piscataway, NJ (1991), p. 3198–3200.

[2] W. B. Haynes, B. Rusnak, K. C. D. Chan, F. Krawczyk, A. Shapiro, R. Bibeau, B. Gentzlinger, D. Montoya, and H. Safa, "Medium-Beta Superconducting Cavity Tests at Los Alamos National Lab for High-Current, Proton Accelerators," in *Proceedings of the Eighth Workshop on RF Superconductivity, Abano Terme, Italy, 1997*, V. Palmieri and A. Lombardi, Editors, LNL, Legnaro, Italy (1998), LNL-INFN (Rep) 133/98, p. 523–533.

[3] Kenji Saito, Shuichi Noguchi, Hitoshi Inoue, Masaaki Ono, Toshio Shishido, Yoshishige Yamazaki, Nobuo Ouchi, Jyoichi Kusano, Motoharu Mizumoto, and Masanori Matsuoka, "Development of 1.3 GHz Medium-β Structure with High Gradient," in *Proceedings of the Eighth Workshop on RF Superconductivity, Abano Terme, Italy, 1997*, V. Palmieri and A. Lombardi, Editors, LNL, Legnaro, Italy (1998), LNL-INFN (Rep) 133/98, p. 534–539.

[4] Nobuo Ouchi, Joichi Kusano, Nobuo Akaoka, Suehiro Takeuchi, Kazuo Hasegawa, Motoharu Mizumoto, Hitoshi Inoue, Eiji Kako, Shuichi Noguchi, Masaaki Ono, Kenji Saito, Toshio Shishido, Ken Mukugi, and Yoichiro Honda, "Development of Superconducting Cavities for High Intensity Proton Accelerator at JAERI," *IEEE Trans. Appl. Superconduct.* **9**, no. 2, p. 1030–1035 (June 1999).

[5] J. L. Biarrotte, H. Safa, J. P. Charrier, S. Jaidane, H. Gassot, T. Junquera, J. Lesrel, G. Ciovati, P. Pierini, D. Barni, and C. Pagani, "704 MHz Superconducting Cavities for a High Intensity Proton Accelerator," in *Proceedings of the 9th Workshop on RF Superconductivity, Santa Fe, NM, 1999*, LANL, Los Alamos, New Mexico (2000), LA-13782-C, p. 384–389.

[6] S. Bauer, W. Diete, B. Griep, M. Peiniger, M. Pekeler, H. Vogel, P. vom Stein, W. Bräutigam, E. Chiaveri, and R. Losito, "Engineering and Fabrication of a Low β Prototype Superconducting Accelerator Module for Forschungszentrum Jülich," in *Proceedings of the 9th Workshop on RF Superconductivity, Santa Fe, NM, 1999*, LANL, Los Alamos, New Mexico (2000), LA-13782-C, p. 443–445.

[7] N. Akaoka, E. Chishiro, K. Hasegawa, M. Mizumoto, J. Kusano, N. Ouchi, H. Inoue, E. Kako, S. Noguchi, M. Ono, K. Saito, T. Shishido, K. Mukugi, C. Tsukishima, O. Takeda, and M. Matsuoka, "Superconducting Cavity Development for High Intensity Proton Linac in JAERI," in *Proceedings of the 9th Workshop on RF Superconductivity, Santa Fe, NM, 1999*, LANL, Los Alamos, New Mexico (2000), LA-13782-C, p. 450–458.

[8] E. Chiaveri, R. Losito, S. Calatroni, A. Daccà, Gemme G., R. Parodi, D. Barni, A. Bosotti, C. Pagani, and G. Varisco, "Production and Test of the Prototype $\beta = 0.85$ Five Cell Cavity for the TRASCO Project," in *Proceedings of the 9th Workshop on RF Superconductivity, Santa Fe, NM, 1999*, LANL, Los Alamos, New Mexico (2000), LA-13782-C, p. 512–515.

[9] T. Tajima, K. C. D. Chan, R. C. Gentzlinger, W. B. Haynes, J. P. Kelley, F. L. Krawczyk, M. A. Madrid, D. I. Montoya, D. L. Schrage, A. H. Shapiro, and J. Mammosser, "Developments of 700-MHz 5-Cell Superconducting Cavities for APT," in *Proceedings of the 2001 Particle Accelerator Conference, Chicago, IL*, P. Lucas and S. Webber, Editors, IEEE, Piscataway, NJ (2001), p. 1119–1121.

[10] C. Pagani, D. Barni, G. Bellomo, A. Bosotti, P. Michelato, R. Paulon, P. Pierini, D. Sertore, and G. Varisco, "Status of the High Energy SC Linac for the TRASCO Program," in *Proceedings of the 2001 Particle Accelerator Conference, Chicago, IL*, P. Lucas and S. Webber, Editors, IEEE, Piscataway, NJ (2001), p. 3612–3614.

[11] G. Ciovati, P. Kneisel, K. Davis, K. Macha, and J. Mammosser, "Superconducting Prototype Cavities for the Spallation Neutron Source (SNS) Project," in *Proceedings of EPAC 2002 Paris: Eighth European Particle Accelerator Conference*, T. Garvey, J. Le Duff, P. Le Roux, Ch. Petit-Jean-Genaz, J. Poole, and L. Rivkin, Editors, EPS-IGA/CERN, Geneva, Switzerland (2002), p. 2247–2249.

[12] M. Mizumoto, N. Ouchi, J. Kusano, E. Chishiro, K. Hasegawa, N. Akaoka, K. Saito, S. Noguchi, E. Kako, H. Inoue, T. Shishido, M. Ono, K. Mukugi, C. Tsukishima, O. Takeda, and M. Matsuoka, "Development of Superconducting Linac for the KEK/JAERI Joint Project," in *Proceedings of the XX International Linac Conference, Monterey, CA*, Alexander W. Chao, Editor, SLAC, Stanford, California (2000), SLAC-R-561, p. 566–568.

[13] K. C. D. Chan, Henri Safa, C. Pagani, and M. Mizumoto, "Review of Superconducting RF Technology for High-Power Proton Linacs," in *Proceedings of the 9th Workshop on RF Superconductivity, Santa Fe, NM, 1999*, LANL, Los Alamos, New Mexico (2000), LA-13782-C, p. 465–471.

[14] A. Facco, "High Intensity Proton Sources," in *Proceedings of SRF 2003: 11th Workshop on RF-Superconductivity: Travemünde, Germany*, DESY, Hamburg, Germany (2004), invited talk.

[15] T. L. Grimm, W. Hartung, T. Kandil, H. Khalil, J. Popielarski, C. Radcliffe, J. Vincent, and R. C. York, "Measurement and Control of Microphonics in High Loaded-Q Superconducting RF Cavities," in *Proceedings of the XXII International Linear Accelerator Conference, Lübeck, 2004*, DESY, Hamburg, Germany (2004), p. 763–765.

[16] T. Kandil, T. L. Grimm, W. Hartung, H. K. Khalil, J. Popielarski, J. Vincent, and R. C. York, "Adaptive Feedforward Cancellation of Sinusoidal Disturbances in Superconducting RF Cavities," in *Proceedings of the XXII International Linear Accelerator Conference, Lübeck, 2004*, DESY, Hamburg, Germany (2004), p. 447–449.

[17] C. C. Compton, T. L. Grimm, W. Hartung, H. Podlech, R. C. York, G. Ciovati, P. Kneisel, D. Barni, C. Pagani, and P. Pierini, "Niobium Cavity Development for the High-Energy Linac of the Rare Isotope Accelerator," in *Proceedings of the 2001 Particle Accelerator Conference, Chicago, IL*, P. Lucas and S. Webber, Editors, IEEE, Piscataway, NJ (2001), p. 1044–1046.

[18] Terry Grimm, Walter Hartung, Holger Podlech, and R. C. York, "Superconducting RF Activities at NSCL," in *Proceedings of the Tenth Workshop on RF Superconductivity, Tsukuba, 2001*, S. Noguchi, Editor, KEK, Tsukuba, Japan (2003), KEK Proceedings 2003-2 A, p. 86–90.

[19] W. Hartung, C. C. Compton, T. L. Grimm, R. C. York, G. Ciovati, and P. Kneisel, "Status Report on Multi-Cell Superconducting Cavity Development for Medium-Velocity Beams," in *Proceedings of the 2003 Particle Accelerator Conference, Portland, OR*, Joe Chew, Peter Lucas, and Sara Webber, Editors, IEEE, Piscataway, NJ (2003), p. 1362–1364.

[20] C. C. Compton, T. L. Grimm, W. Hartung, H. Podlech, R. C. York, G. Giovati, P. Kneisel, D. Barni, C. Pagani, and P. Pierini, "Prototyping of a Multicell Superconducting Cavity for Acceleration of Medium-Velocity Beams," *Phys. Rev. ST Accel. Beams* **8**, 042003 (April 2005).

[21] T. L. Grimm, W. Hartung, M. Johnson, R. C. York, P. Kneisel, and L. Turlington, "Cryomodule Design for the Rare Isotope Accelerator," in *Proceedings of the 2003 Particle Accelerator Conference, Portland, OR*, Joe Chew, Peter Lucas, and Sara Webber, Editors, IEEE, Piscataway, NJ (2003), p. 1350–1352.

[22] T. L. Grimm, S. Bricker, C. Compton, W. Hartung, M. Johnson, F. Marti, J. Popielarski, R. C. York, G. Ciovati, P. Kneisel, and L. Turlington, "Experimental Study of an 805 MHz Cryomodule for the Rare Isotope Accelerator," in *Proceedings of the XXII International Linear Accelerator Conference, Lübeck, 2004*, DESY, Hamburg, Germany (2004), p. 773–775.

[23] D. Barni, G. Ciovati, P. Kneisel, C. Pagani, P. Pierini, and P. Ylae-Oijala, "A $\beta_g = 0.472$ Cavity for RIA: A Proposal," Tech Note JLab-TN-01-014, Jefferson Lab, Newport News, Virginia (2001).

[24] B. Aune, R. Bandelmann, D. Bloess, B. Bonin, A. Bosotti, M. Champion, C. Crawford, G. Deppe, B. Dwersteg, D. A. Edwards, H. T. Edwards, M. Ferrario, M. Fouaidy, P.-D. Gall, A. Gamp, A. Gössel, J. Graber, D. Hubert, M. H"uning, M. Juillard, T. Junquera,

H. Kaiser, G. Kreps, M. Kuchnir, R. Lange, M. Leenen, M. Liepe, L. Lilje, A. Matheisen, W.-D. Möller, A. Mosnier, H. Padamsee, C. Pagani, M. Pekeler, H.-B. Peters, O. Peters, D. Proch, K. Rehlich, D. Reschke, H. Safa, T. Schilcher, P. Schmüser, J. Sekutowicz, S. Simrock, W. Singer, M. Tigner, D. Trines, K. Twarowski, G. Weichert, J. Weisend, J. Wojtkiewicz, S. Wolff, and K. Zapfe, "Superconducting TeSLA cavities," *Phys. Rev. ST Accel. Beams* **3**, 092001 (2000).

[25] K. Halbach and R. F. Holsinger, "SUPERFISH—A Computer Program for Evaluation of RF Cavities with Cylindrical Symmetry," *Part. Accel.* **7**, p. 213–222 (1976).

[26] James H. Billen and Lloyd M. Young, "POISSON/SUPERFISH on PC Compatibles," in *Proceedings of the 1993 Particle Accelerator Conference, Washington, DC*, Steven T. Corneliussen, Editor, IEEE, Piscataway, NJ (1993), p. 790–792.

[27] T. L. Grimm, W. Hartung, F. Marti, H. Podlech, R. C. York, J. Popielarski, C. Wiess, L. Kempel, G. Ciovati, and P. Kneisel, "Input Coupling and Higher-Order Mode Analysis of Superconducting Axisymmetric Cavities for the Rare Isotope Accelerator," in *Proceedings of EPAC 2002 Paris: Eighth European Particle Accelerator Conference*, T. Garvey, J. Le Duff, P. Le Roux, Ch. Petit-Jean-Genaz, J. Poole, and L. Rivkin, Editors, EPS-IGA/CERN, Geneva, Switzerland (2002), p. 2241–2243.

[28] D. G. Myakishev and V. P. Yakovlev, "An Interactive Code SUPERLANS for Evaluation of RF-Cavities and Acceleration Structures," in *Conference Record of the 1991 IEEE Particle Accelerator Conference, San Francisco, CA*, Loretta Lizama and Joe Chew, Editors, IEEE, Piscataway, NJ (1991), p. 3002–3004.

[29] Hasan Padamsee, Jens Knobloch, and Tom Hays, *RF Superconductivity for Accelerators*, John Wiley & Sons, New York (1998).

[30] X. Wu, G. Gorelov, T. Grimm, W. Hartung, F. Marti, and R. C. York, "The Beam Dynamics Studies of Combined Misalignments and RF Errors for RIA," in *Proceedings of the 2003 Particle Accelerator Conference*, Joe Chew, Peter Lucas, and Sara Webber, Editors, IEEE, Piscataway, New Jersey (2003), p. 2972–2974.

[31] K. M. Wilson, I. E. Campisi, E. F. Daly, G. K. Davis, M. Drury, J. E. Henry, P. Kneisel, G. Myneni, T. Powers, W. J. Schneider, M. Stirbet, Y. Kang, K. Cummings, and T. Hardek, "The Prototype Fundamental Power Coupler for the Spallation Neutron Source Superconducting Cavities: Design and Initial Test Results," in *Proceedings of the Tenth Workshop on RF Superconductivity: Tsukuba, 2001*, S. Noguchi, Editor, KEK, Tsukuba, Japan (2003), KEK Proceedings 2003-2 A, p. 535–539.

[32] Quan-Sheng Shu, Joe Susta, Guangfeng Cheng, Steven Einarson, Todd. A. Treado, William C. Guss, and Michael Tracy, "Design and Fabrication of Input RF Coupler Windows for the SNS," Presented at the Workshop on High-Power Couplers for Superconducting Accelerators (30 October–1 November 2002, Jefferson Lab, Newport News, VA).

[33] Quan-Sheng Shu, Joe Susta, Guangfeng Cheng, T. L. Grimm, John Popielarski, Steven Einarson, and Todd A. Treado, "Design and Fabrication of Input RF Coupler Windows for the U.S. Rare Isotope Project (RIA)," in *Proceedings of SRF 2003: 11th Workshop on RF-Superconductivity: Travemünde, Germany*, DESY, Hamburg, Germany (2004), Paper ThP35.

[34] M. Stirbet, J. Popielarski, T. L. Grimm, and M. Johnson, "RF Conditioning and Testing of Fundamental Power Couplers for the RIA Project," in *Proceedings of SRF 2003: 11th Workshop on RF-Superconductivity: Travemünde, Germany*, DESY, Hamburg, Germany (2004), Paper ThP26.

[35] W. Hartung, F. Krawczyk, and H. Padamsee, "Studies of Multipacting in Axisymmetric Cavities for Medium-Velocity Beams," in *Proceedings of the Tenth Workshop on RF Superconductivity, Tsukuba, 2001*, S. Noguchi, Editor, KEK, Tsukuba, Japan (2003), KEK Proceedings 2003-2 A, p. 627–631.

[36] J. Hogan, G. Ciovati, D. Machie, J. Pitts, J. Preble, W. J. Schneider, K. Smith, L. Turlington, K. Matsumoto, and R. Mitchell, "Design of the SNS Cavity Support Structure," in *Proceedings of the 2001 Particle Accelerator Conference, Chicago, IL*, P. Lucas and S. Webber, Editors, IEEE, Piscataway, NJ (2001), p. 1158–1159.

[37] John Popielarski, "RF Controls and Microphonic Measurements of the $\beta = 0.47$ Elliptical Test Module," Technical report, NSCL, Michigan State University, East Lansing, Michigan (October 2007), final report for Department of Energy Grant DE-FG02-07ER41461.